Biointerface Research in Applied Chemistry
Open-Access Journal (ISSN: 2069-5837)

Article
Volume 13, Issue 3, 2023, 248
https://doi.org/10.33263/BRIAC133.248

Vibrational Study of Mono and Diprotonated Species of Potent Anti-acid Ranitidine Hydrochloride Combining DFT with SQMFF Calculations

Davide Romani [1], Maria J. Márquez [2], Silvia Antonia Brandán [2,*]

[1] Dipartimento di Scienze Mediche Chirurgiche e Neuroscienze, Università degli Studi di Siena, Via Banchi di Sotto 55 (53100), Siena, Italia; dromaniti@gmail.com (D.R.);
[2] Cátedra de Química General, Instituto de Química Inorgánica, Facultad de Bioquímica, Química y Farmacia, Universidad Nacional de Tucumán, Ayacucho 471, (4000), San Miguel de Tucumán, Tucumán, Argentina
* Correspondence: sbrandan@fbqf.unt.edu.ar (S.A.B.);

Scopus Author ID 6602262428
Received: 20.02.2022; Accepted: 6.04.2022; Published: 7.06.2022

Abstract: Structural and vibrational studies of mono (M) and diprotonated (D) species of ranitidine hydrochloride (RH) have been performed by combining B3LYP/6-31G* calculations with the scaled quantum mechanical force field (SQMFF) methodology. Four M structures in the gas phase and aqueous solution and two D *E/Z* and *Z/E* isomers in solution were considered. The M and D free base, cationic, and hydrochloride species show higher dipole moment values and expansion of volumes in solution, while higher solvation energies are predicted for both D (*E/Z*) and (*Z/E*) species. NBO and AIM studies suggest high stabilities of D (*Z/E*) cationic and hydrochloride species in solution. Gap values show that the M and D species are the most reactive in both media. M and two D forms were completely assigned, and their force constants were reported. The D hydrochloride (*E/Z*) form shows two IR bands at 2718 and 2625 cm^{-1} assigned to νN6-H34 and νN5-H44 stretching modes where the formation of O3-H34···N6 bond justifies the strong shifting of νN6-H34 stretching mode towards lower wavenumbers. The IR bands at 2563, 2515, and 2475 cm^{-1} assigned to the two D species, together with the absence of an intense band at 1764 $cm^{-1,}$ show clearly that M species is not present in the solid phase, but the two D hydrochloride (*E/Z*) and (*Z/E*) species.

Keywords: Ranitidine hydrochloride; vibrational spectra; molecular structure; descriptor properties; DFT calculations.

© 2022 by the authors. This article is an open-access article distributed under the terms and conditions of the Creative Commons Attribution (CC BY) license (https://creativecommons.org/licenses/by/4.0/).

1. Introduction

Ranitidine hydrochloride (RH) is a pharmacological drug recommended in October 1984 by the U.S. Food and Drug Administration (FDA) for the treatment and prevention of stomach and duodenum ulcers and the treatment of heartburn, inflammation of the esophagus, and Zollinger-Ellison syndrome because this medicine is a potent inhibitor of gastric acid secretion [1-14]. Recent FDA studies (2019) have evidenced risk to public health due to the presence in some products of the impurity N-Nitrosodimethylamine (NDMA) because when it is present at high levels may increase the risk of cancer in humans [5,12,14,15]. Hence, FDA advises consumers, patients, and health care professionals that this drug should not be available unless its quality can be assured [15]. Therefore, the control of purity of ranitidine hydrochloride is fundamental for that it can be used for the purposes above in form safe and

effective [1-4]. Vibrational spectroscopy is the most simple and quick technique to identify a species, and, so far, there are spectral studies on RH, but the complete assignments of all bands observed in its infrared spectrum, taking into account its experimental structure, was not performed yet either exist vibrational studies for its free base and cationic species [16-18]. Ramesh *et al*. have studied RH's infrared and Raman spectra by using a theoretical structure different from the experimental ones where the group HCl of RH is kinked to O of furan ring instead of N atom belonging to N-$(CH_3)_2$ group. Hence, that proposed assignment is erroneous because the predicted infrared spectrum does not correspond to the experimentally observed structure [18]. Besides, in that investigation, the vibrational assignments of RH were not performed using the normal internal coordinates. The force field was not obtained, and the other two species, free base and cationic species were not studied either in the gas phase or in an aqueous solution. The most important detail to consider in all the hydrochloride species is that cationic species are present in the solution, and, for these reasons, the three species of RH should be studied [19]. On the other hand, Cholerton *et al*. have evidenced an equimolar mixture of *E/Z* and *Z/E* enamine isomers of RH in an aqueous acid medium [20]. Hence, these two diprotonated structures should also be considered in any study related to this species in solution because of the important use of ranitidine as an antiacid drug. Always, comparisons between both experimental and predicted IR spectra together with the application of scaled quantum mechanical force field (SQMFF) methodology and the normal internal coordinates are necessary to perform complete and reliable assignments of all vibration modes present in RH [21,22]. Hence, from the present work, the identifications of mono and diprotonated structures of RH and its free base and cationic species are now possible to control and avoid impurities and falsifications of this important drug. Moreover, predictions of different properties of this drug are very important due to the presence of three donors and seven acceptors groups in the RH structure, as well as the existence of C-N-$(CH_3)_2$ group also present in alkaloids agents, among other drugs [23-26]. This way, this investigation aims to predict the IR and Raman spectra for the mono and diprotonated structures of RH according to the experimental structure determined by X-ray diffraction and, also, the corresponding to its free base cationic species [8-10,20]. The IUPAC name of RH is (*E*)-1-*N*'-[2-[[5-[(dimethylamino)methyl]furan-2-yl]methylsulfanyl]ethyl]-1-*N*-methyl-2-nitroethene-1,1-diamine; hydrochloride while the generic name is Zantac. Theoretical calculations based on the density functional theory (DFT) method have been performed to optimize the initial monoprotonated RH structure taken from the experimental CIF file and its free base and cationic species in the gas phase aqueous solution. After that, their properties and reactivities were predicted by using additional calculations, such as natural bond orbital (NBO), atoms in molecules (AIM) calculations, frontier orbitals, and typical descriptors [27-31]. Finally, comparisons of properties obtained for these mono and diprotonated species of RH with others were performed [23-26].

2. Materials and Methods

The initial monoprotonated structure of RH, in eclipsed conformation and with the protonation at the dimethylamino N atom, was taken from the experimental CIF file reported by Hempel *et al*. [10]. Then the Cl and the H atoms were removed from that structure, respectively to obtain the corresponding to the cationic and free base ones. For such purposes, the *GaussianView* program was employed [32]. Consequently, the structures of the three species were optimized in the gas phase and aqueous solution with the B3LYP/6-31G* method

and the Gaussian 09 program [33-35]. Considering that Cholerton *et al*. has evidenced an equimolar mixture of E/Z and Z/E enamine isomers of diprotonated RH in an aqueous acid medium [20], these two species are found also optimized at the same level of theory together with the corresponding to the free base and cationic species. In solution, the integral equation formalism variant polarised continuum method (IEFPCM) combined with the universal solvation model was used in the optimizations and the determinations of respective solvation energies [36-38]. The volume variations observed in all structures were computed with the Moldraw program [39]. Here, the scaled quantum mechanical force field (SQMFF) methodology was applied together with the normal internal coordinates and scaling factors to obtain the harmonic force fields of all mono and diprotonated species of RH [21]. Hence, the potential energy distributions (PED) were determined with the Molvib program, while in the assignments of all vibration modes, only PED contributions were considered ≥ 10% [22]. Corrections to intensities were performed to the theoretical Raman spectra expressed in activities [40]. Atomic charges, stabilization energies, molecular electrostatic potentials, topological properties, and frontier orbitals were calculated for all RH species in the two media [23-26,41]. The ultraviolet-visible spectra for those species were also predicted in water by using Time-dependent DFT calculations (TD-DFT) at the 6-31G* level of theory with the Gaussian 09 program [34] because this spectroscopy is also employed in the determination of RH of pharmaceutical preparations in aqueous solution [42,43].

3. Results and Discussion

3.1. Optimizations of mono and diprotonates species in different media.

The experimental studies reported by Hempel *et al*. for RH in the solid-state [10] were considered in this work because two possible configurations were observed for the enamine portion of the molecule concerning the C18=C19 double bond; one of them, the *E form* and the other one, *Z*, in which the methylamino and nitro groups are *cis* and *trans* to each other, respectively. Hence, we have considered four conformers of RH in the gas phase where the dimethylamino and nitro groups are *cis* while in three of them, the nitro and methylamino groups are *trans* across the side chain C18=C19 double bond. Therefore, C1, C2, and C3 have *Z form* while C4 has *E form*. These monoprotonated structures can be seen in Figure 1. From the figure, we can see that the dimethylamino and nitro groups are *cis* in the four conformers, and with red circles observed that C1, C2, and C3 forms where the nitro and methylamino groups are *trans* (*Z form)* while in C4 is *Cis* (*E form*). In an aqueous acid medium, Cholerton *et al*. have evidenced an equimolar mixture of *E/Z* enamine isomers of diprotonated RH in solution [20]. The scheme of protonation proposed by Cholerton *et al*. for the nitroethene group of RH in an aqueous acid medium can be seen in Figure S1. According to that scheme, four theoretical geometrical diprotonated isomers are possible, *Z/Z*, *E/Z*, *Z/E*, and *E/E*, but only they have demonstrated the presence of an equimolar mixture of diprotonated *E/Z* and *Z/E* enamine isomers. The existence of other isomers is highly unlikely by the steric effect and possibly also the lack of hydrogen bonding possibilities for the *Z/Z* isomer [20]. Hence, those four monoprotonated conformations presented in Fig. 1 were also optimized in an aqueous solution in addition to the diprotonated *E/Z* and *Z/E* isomers observed in Figure 2. In Table 1 are summarized calculated total and relative energies, dipolar moments, volumes, and populations expressed in percentages for all mono and diprotonated species of RH in both media by using the B3LYP/6-31G* method.

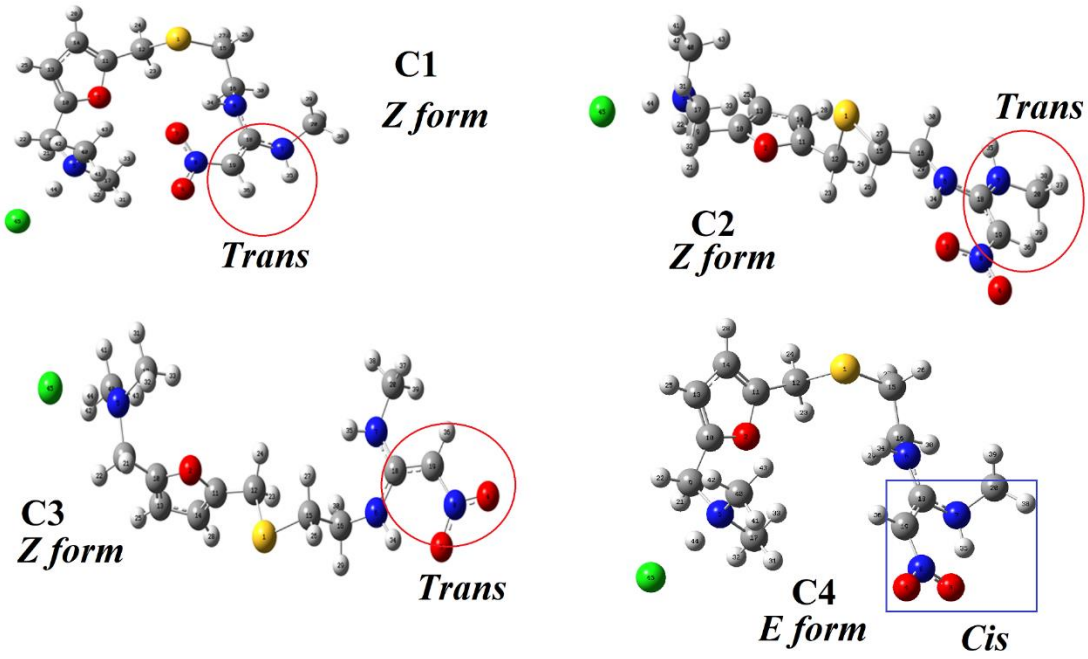


Figure 1. Molecular monoprotonated structures of ranitidine hydrochloride and atoms numbering.

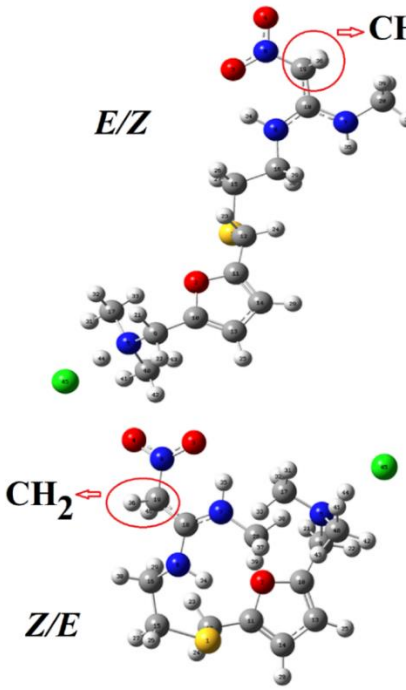


Figure 2. Molecular diprotonated structures of ranitidine hydrochloride and atoms numbering.

The variations that present those monoprotonated species in dipolar moments, volumes, and populations can be seen in Figure 3. Analyzing these results, we observed that the optimized monoprotonated RH structure had eclipsed conformation, and the dimethylamino N atom is protonated. Then, C1 is the most stable conformer in the gas phase with higher dipole moment and population values, but its form presents a lower volume, as shown in Figure 3. The differences in the energies values evidence that the monoprotonated C1 structure of RH is present in the gas phase and, for this reason, the properties only for this conformer and for its free base and cationic species were calculated in the gas phase.

Table 1. Calculated total (*E*) and relative energies (Δ*E*), dipolar moment (μ), volume (V), and population values of mono and diprotonated ranitidine hydrochloride in the gas phase and aqueous solution by using the B3LYP/6-31G* method.

B3LYP/6-31G*METHOD					
MONOPROTONATED HYDROCHLORIDE					
GAS PHASE					
Conformers	*E* (Hartrees)	*ΔE* (kJ/mol)	*μ* (Debye)	V (Å^3)	Population %
C1 (*Z form*)	-1812.1781	0.00	17.41	365.4	67.38
C2(*Z form*)	-1812.1768	-3.41	13.05	365.5	15.85
C3(*Z form*)	-1812.1749	-8.39	7.87	366.2	3.29
C4 (*E form*)	-1812.1766	-3.93	16.97	374.9	13.48
AQUEOUS SOLUTION					
C1 (*Z form*)	-1812.2331	-9.70	24.67	369.6	1.00
C2(*Z form*)	-1812.2368	0.00	21.25	356.7	52.00
C3(*Z form*)	-1812.2367	-0.26	14.75	370.8	47.00
C4 (*E form*)	-1812.2312	-14.69	26.52	373.5	0.15
DIPROTONATED HYDROCHLORIDE					
GAS PHASE					
E/Z(C2)	-1812.7453	0.00	14.63	360.6	98.00
Z/E(C4)	-1812.7416	-9.70	16.14	378.0	2.00
AQUEOUS SOLUTION					
E/Z(C2)	-1812.8022	-34.62	20.83	363.4	0.00
Z/E(C4)	-1812.8154	0.00	25.92	371.1	100

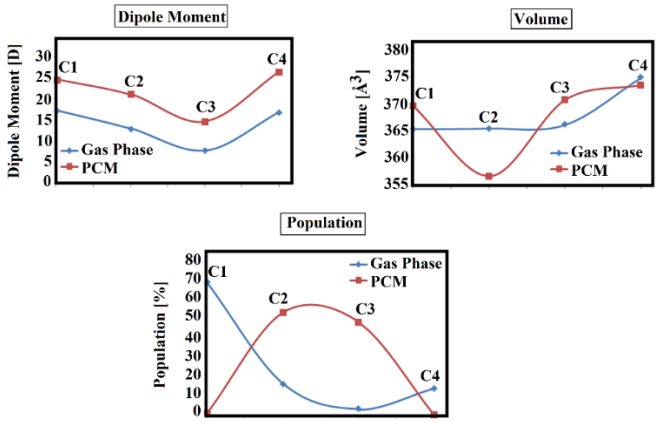


Figure 3. Dipole moments, volumes, and populations of four monoprotonated species of ranitidine hydrochloride in the gas phase and aqueous solution using the B3LYP/6-31G* level.

A quick observation shows that RH presents high hydration in solution, probably due to its high dipole moment values in all conformations. C1 shows the expansion of volume in solution while C4 contraction of volume in this medium. In an aqueous solution, the monoprotonated C2 and C3 forms present the higher populations while the other two practices are not present in the solution. Note that the diprotonated species *E/Z* and *Z/E* isomers of RH are also presented in Table 1. Analyzing the exhaustively results for these diprotonated species, we observed that the E/Z isomer of RH is the most stable in the gas phase with a higher population, while in solution, the Z/E isomer presents the solution higher population and, in addition, is the most stable. Hence, taking into account the studies performed by Hempel *et al.* in the solid phase RH is a monoprotonated species [10], as C1 in the gas phase, while in solution, RH is a diprotonated species in an equimolar mixture of *E/Z* enamine isomers, as evidenced by Cholerton *et al*. [20]. Thus, in this work, the properties of monoprotonated C1

structure of RH in the gas phase and solution are studied together with the diprotonated *(E/Z)* in the gas phase and *(Z/E)* in solution because both have higher populations. The same parameters calculated for RH are predicted for the mono and diprotonated free base and cationic species of RH; these results are presented in Table 2. The optimizations of all mono and diprotonated species produce positive frequencies confirming the natures of the reached stationary points except for diprotonated cationic *(Z/E)* species in solution that shows two imaginary frequencies. This latter result indicates that diprotonated cationic *(Z/E)* species in solution is an unstable species. Regarding first the monoprotonated free base and cationic species, it is observed that the cationic species increase its dipole moment and volume in solution, as expected because it is a charged species that is hydrated in this medium, while the free base also increases both parameters due to the protonation but a greater change in the volume is observed in this species (ΔV= 5.6 Å^3), as compared with the cationic one (ΔV= 2.0 Å^3).

Table 2. Calculated total (*E*) and relative energies (ΔE), dipolar moment (μ), and volume (V) values of mono and diprotonated free base and cationic species of ranitidine hydrochloride in the gas phase and aqueous solution by using the B3LYP/6-31G* method.

B3LYP/6-31G*METHOD				
MONOPROTONATED				
GAS PHASE				
Species	*E* (Hartrees)	E_{ZPVE} (Hartrees)	μ (Debye)	V (Å^3)
Cationic (C1)	-1351.7628	-1351.3875	5.40	340.9
Free Base (C1)	-1351.3603	-1351.0020	8.07	338.6
AQUEOUS SOLUTION				
Cationic(C1)	-1351.8563	-1351.4804	13.72	342.9
Free Base (C1)	-1351.3914	-1351.0328	11.48	344.2
DIPROTONATED				
GAS PHASE				
Cationic *(E/Z)*	-1352.3505	-1351.9669	5.49	343.2
Free Base *(E/Z)*	-1351.9242	-1351.5562	7.57	338.5
Cationic *(Z/E)*	-1352.3315	-1351.9458	4.86	343.9
Free Base *(Z/E)*	-1351.9187	-1351.5495	5.67	348.8
AQUEOUS SOLUTION				
Cationic *(E/Z)*	-1352.4517	-1352.0655	4.46	341.8
Free Base *(E/Z)*	-1351.9579	-1351.5889	11.88	335.5
Cationic *(Z/E)*[#]	-1352.3177	-1351.9329	7.76	349.2
Free Base *(Z/E)*	-1351.9700	-1351.5984	14.14	347.0

[#]Imaginary frequencies

The two diprotonated free base and cationic species *(E/Z)* are most stable in the gas phase, while in solution are most stable the *(Z/E)* ones, as evidenced in Table 4. Figure 4 shows the variations in dipolar moments and volumes that present these two diprotonated species of RH. When the dipole moments of two diprotonated species are analyzed, we observed that the free base *(E/Z)* in the gas phase presents a higher dipole moment than the form *(Z/E)* while, on the contrary, it is observed in solution. Similar behaviors are observed in the dipole moments of both cationic *(E/Z)* and *(Z/E)* species. Here, a very important result is that both diprotonated free base species have higher dipole moments than the cationic ones in the two media. The free base *(Z/E)* in the solution has a higher value than the *(E/Z)* one. Analyzing the volumes, the

free bases (Z/E) in both media have higher volumes than the other ones if the cationic (*Z/E)* in solution is not considered due to the imaginary frequencies.

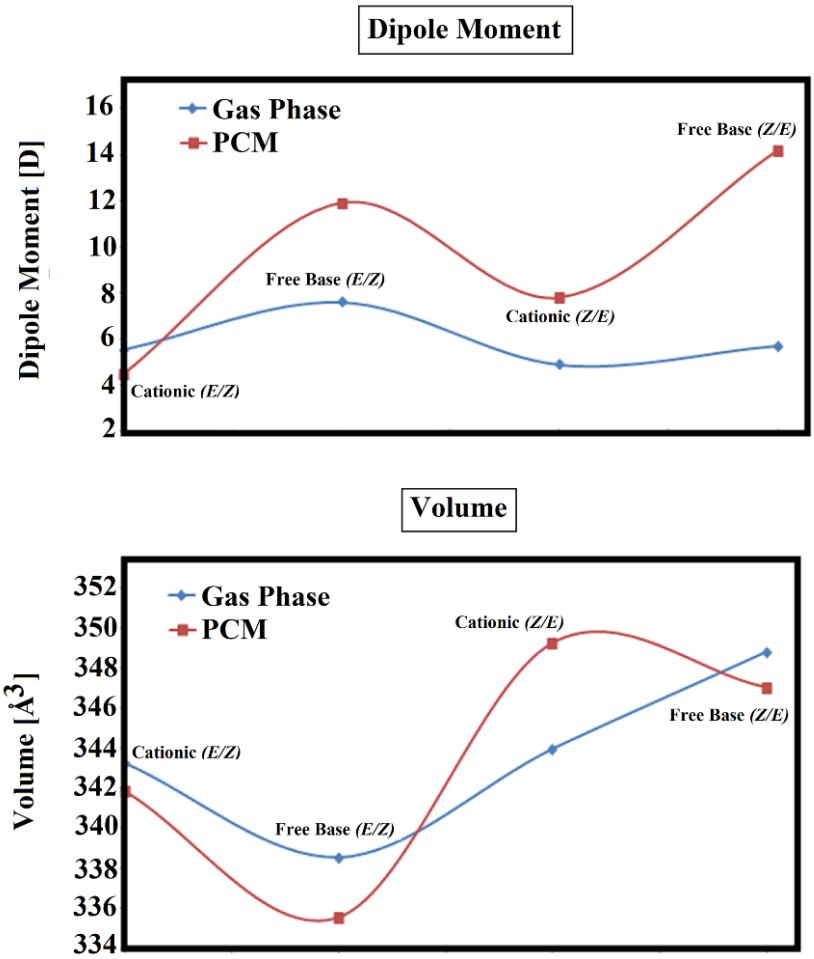


Figure 4. Dipole moments and volumes of diprotonated free base and cationic species of ranitidine hydrochloride in the gas phase and aqueous solution using the B3LYP/6-31G* level of theory.

3.2. Solvation energies of mono and diprotonated species.

Table 3 shows corrected solvation energies (ΔG_c) by the total non-electrostatic terms (ΔG_{ne}) of mono and diprotonated free base, cationic, and hydrochloride species of ranitidine in an aqueous solution by using the B3LYP/6-31G* method while in Figure 5 are observed the profiles that present the corrected values. The uncorrected value (ΔG_{un}) is determined directly from the energy difference between the value in the solution and the corresponding gas phase. Fig. 5 shows clearly that the mono and diprotonated free base *(E/Z)* species have approximately the same values (-105.69 and -104.61 kJ/mol) but are different from the diprotonated *(Z/E)* species (-147.68 kJ/mol) while the diprotonated cationic *(E/Z)* presents a more negative value (295.67 kJ/mol) than the monoprotonated one (281.45 kJ/mol). Analyzing the values of hydrochloride species, it is observed that the diprotonated *(Z/E)* species has a higher value (-224.38 kJ/mol) than the mono and diprotonated *(E/Z)* one (-179.87 and -184.03 kJ/mol). These results clearly evidence that the three diprotonated species of RH present higher solvation energies than the monoprotonated ones. Hence, the presence of CH_2 groups in all of them improves the hydration in an aqueous solution.

Table 3. Corrected solvation energies by the total non-electrostatic terms of mono and diprotonated ranitidine in an aqueous solution by using the B3LYP/6-31G* method.

MONOPROTONATED RANITIDINE[a]			
Solvation energy (kJ/mol)			
Condition	ΔG_{un}	ΔG_{ne}	ΔG_{c}
B3LYP/6-31G* method			
Free base	-81.57	24.12	-105.69
Cationic	-245.25	36.20	-281.45
Hydrochloride	-144.26	35.61	-179.87
DIPROTONATED RANITIDINE[a]			
Free base (*E*/*Z*)	-88.39	16.22	-104.61
Free base (*Z*/*E*)	-134.56	13.12	-147.68
Cationic (*E*/*Z*)	-265.45	30.22	-295.67
Hydrochloride (*E*/*Z*)	-149.25	34.78	-184.03
Hydrochloride (*Z*/*E*)	-193.57	30.81	-224.38

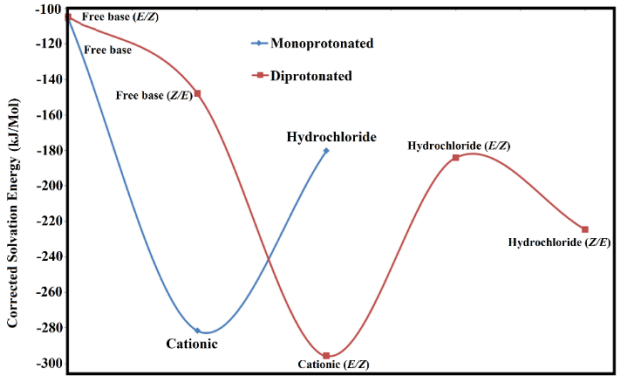


Figure 5. Corrected solvation energy values of mono and diprotonated free base, cationic, and hydrochloride species of ranitidine using the B3LYP/6-31G* level of theory.

3.3. Geometrical parameters of mono and diprotonated species.

Table 4 are presented the geometrical parameters of monoprotonated C1 structures of the free base, cationic, and hydrochloride species of RH in the gas phase compared with the corresponding to the diprotonated (*E/Z)* and (*Z/E)* species in solution, as evidenced by Cholerton *et al*. [20]. For a quick evaluation of the results, the values were compared with the experimental ones reported for the monoprotonated species of RH by Hempel *et al*. [10] by means of the root-mean-square deviation (RMSD).

Hence, better correlations (0.028-0.026 Å and 2.7-1.6º for bond lengths and angles, respectively) are observed for those three species in the gas phase where the dimethylamino and nitro groups are in *cis* positions, but the nitro group concerning methylamino group in *trans* position, as shown in Figure 1, while for the diprotonated forms the values increase to 0.049-0.046 Å and 7.0-6.3º for bond lengths and angles, respectively. However, the calculated dihedral angles for mono and diprotonated species undergo important changes in both media compared with the experimental values, although the lower RMSDs values are predicted for the monoprotonated cationic and hydrochloride species of RH. The structures of diprotonated (*E/Z)* and (*Z/E)* species are different from the monoprotonated ones because in the diprotonated species, the double C=C bonds change to simple with the addition of H atoms and formations of new N-CH_2 groups. For these reasons, changes in the RMSDs values of all diprotonated species of RH in solution are expected. Moreover, another very interesting result is observed for the diprotonated three (*E/Z)* species of RH in solution because due to the proximities

between the N-H and NO_2 groups (See fig. 2), the calculations have optimized the nitro groups of free base and hydrochloride species protonated, as HO-N-O. These protonations in those two species were not mentioned by Cholerton *et al*. in the scheme of protonation proposed for the nitroethene group of RH [43], as shown in Figure S1.

Table 4. Comparison of calculated geometrical parameters of mono and diprotonated free base, cationic, and hydrochloride species of ranitidine in the gas phase and aqueous solution compared with those experimental ones.

Parameter	B3LYP/6-31G* Method[a]									Exp.,[b]
	GAS PHASE			AQUEOUS SOLUTION						
	Monoprotonated			Diprotonated (*E/Z*)			Diprotonated (*Z/E*)			
	Free base	Cationic	HCl	Free base	Cationic	HCl	Free base	Cationic	HCl	
Bond lengths (Å)										
S1-C12	1.863	1.858	1.863	1.862	1.859	1.860	1.867	1.864	1.865	1.833
S1-C15	1.839	1.837	1.838	1.834	1.831	1.834	1.840	1.840	1.840	1.807
O2-C10	1.368	1.371	1.372	1.381	1.379	1.379	1.382	1.379	1.379	1.379
O2-C11	1.372	1.369	1.370	1.379	1.377	1.376	1.376	1.371	1.373	1.375
N5-C9	1.460	1.541	1.502	1.478	1.518	1.518	1.480	1.531	1.519	1.510
N5-C17	1.459	1.508	1.485	1.464	1.491	1.491	1.465	1.499	1.492	1.485
N5-C18	1.457	1.508	1.486	1.464	1.494	1.491	1.462	1.496	1.490	1.455
N6-C16	1.453	1.466	1.465	1.458	1.467	1.458	1.472	1.472	1.471	1.450
N6-C19	1.372	1.356	1.361	1.297	1.327	1.297	1.324	1.324	1.324	1.332
N7-C19	1.350	1.359	1.372	1.354	1.321	1.353	1.328	1.328	1.328	1.335
N7-C21	1.448	1.461	1.462	1.460	1.466	1.460	1.460	1.459	1.460	1.450
N8-C20	1.393	1.377	1.394	1.470	1.473	1.471	1.487	1.486	1.485	1.348
C19=C20	1.396	1.407	1.392	1.526	1.517	1.526	1.505	1.506	1.506	1.425
RMSD	**0.028**	**0.026**	**0.026**	**0.048**	**0.046**	**0.048**	**0.048**	**0.049**	**0.048**	
Bond angles (º)										
C12-S1-C15	101.0	102.9	101.7	100.7	101.4	100.3	101.0	101.0	101.4	102.0
C16-N6-C18	123.1	124.9	123.4	119.0	126.6	119.1	125.6	125.7	125.7	127.4
N6-C18-N7	116.8	119.7	118.5	125.8	123.0	125.9	121.8	121.7	121.9	120.9
N8-C19-C18	124.1	124.7	124.7	112.0	110.1	112.1	108.6	109.1	108.8	123.9
C18-N7-C20	124.9	125.4	123.7	126.0	125.7	125.9	124.2	124.3	124.3	123.7
RMSD	**2.7**	**1.6**	**2.1**	**7.0**	**6.3**	**6.9**	**6.9**	**6.7**	**6.8**	
Dihedral angles (º)										
O-C-C-S	-80.2	-110.5	-98.1	-78.6	-83.9	-75.2	-75.3	-71.6	-74.0	-66.0
N-C-C-S	-54.8	-49.4	-56.2	177.8	-159.8	179.5	-62.6	-63.1	-62.1	173.0
O-N-C-C	-178.7	173.6	171.1	177.8	74.3	59.3	74.5	76.8	75.0	178.1
N-C-C-N	-178.7	-166.8	-167.5	162.2	145.2	160.1	-108.3	-107.9	-	-175.0
RMSD	**211.8**	**113.5**	**115.8**	**168.7**	**236.8**	**177.9**	**133.0**	**132.8**	**132.5**	

[a]This work, [b]Ref [10]

Thus, the different intra-molecular interactions in the three diprotonated (*E/Z)* species are observed in Figure 6. In the free base is observed the O3-H34···N6 interaction; in the cationic species are observed two N6-H34···O3 and N5-H44···O4 interactions and, in the hydrochloride species, the N5-H44···Cl45 and O3-H34···N6 interactions. These interactions confer to these species higher stabilities in solution. In the diprotonated (*Z/E)* species, the only interaction observed is the expected N5-H44···Cl45 for the hydrochloride one. The calculations predicted notable changes in the dihedral angles of all species of RH and, in particular, in the side chains related to the methylamino and nitro groups; those angles are: O2-C11-C12-S1, N6-C16-C15-S1, O4-N8-C19-C18, and N8-C19-C18-N7 dihedral angles. Finally, taking into account the relatively low RMSD values predicted for bond lengths and angles in all structures of RH in this work, the analyses vibrational will be performed for both mono and diprotonated structures of this antiacid agent.

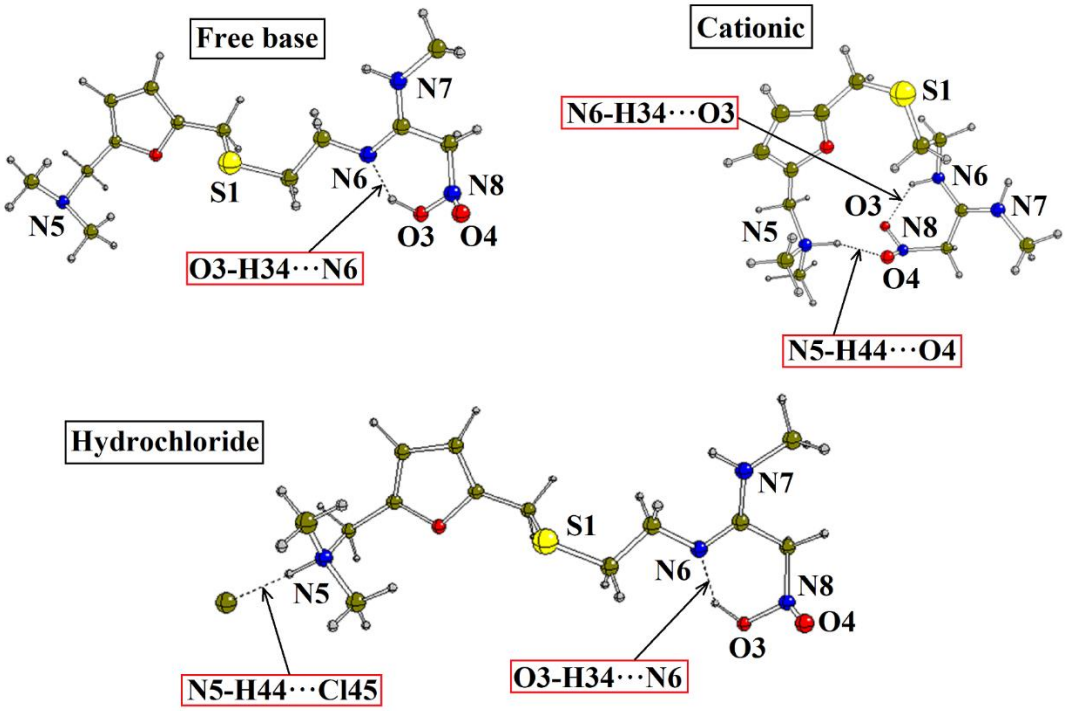


Figure 6. Diprotonated (*E/Z*) structures of the free base, cationic, and hydrochloride species of ranitidine hydrochloride show the formation of H bonds.

3.4. Atomic charges and molecular electrostatic potentials of monoprotonated species.

The calculations of atomic charges and molecular electrostatic potentials (MEP) and the evaluations of these parameters are essential in both mono and diprotonated species of RH due to the presence of acceptors atoms (N and O) and donors N-$(CH_3)_2$, N-CH_3 and NO_2 groups that are of importance for the localization of most reactive sites nucleophilic and electrophilic and, also, for the stabilities of these species in different media. Thus, atomic charges and MEPs were calculated only for the eight most important atoms in the mentioned groups (S1, O2, O3, O4, N5, N6, N7, and N8). The O2 belongs to the furan ring, N8, O3, and O4 belong to the nitro group, while N5 belongs to dimethyamino and N7 to methylamino. In Table S1 are summarized three different atomic charges, Merz-Kollman (MK), Mulliken, and natural population (NPA), together with the MEPs values for the monoprotonated free base, cationic and hydrochloride species of RH in gas and aqueous solution by using the B3LYP/6-31G* method. In Figure S2 are presented the behaviors of those three charges on the S1, O2, O3, O4, N5, N6, N7, and N8 atoms of the monoprotonated free base, cationic, and hydrochloride species in both media. The similar curves of Mulliken and NPA charges on all atoms (red and green lines, respectively) observed for the cationic and hydrochloride species in both media reveal the same behaviors of those two species, and only slight variations are evidenced in the Mulliken charge on N5 of the free base because these charges are less negative than the NPA ones. The most important results are observed in the different MK charges predicted on all atoms (blue line) of the three species and, in particular, the charges on N5 of cationic and hydrochloride species in both media are positive, while in the free base species, all charges on N atoms are negative except for N8 that in the three studied charges show positive values, having the higher value the MK charge.

If now the MEP values are analyzed from Table S1, we observed the typically expected tendency due to the different electronegativities, which are: S > O > N while if the mapped MEP surfaces are graphed with the *GaussView* program, the different colorations that

present these surfaces are shown in Figure S3. In the free base, a strong red coloration is observed on the NO_2 group, while in the hydrochloride form, the intense red color is observed on the Cl atom. These sites are nucleophilic places, while in those two species, the blue colors are shown on the N-H groups indicating electrophilic sites. In the cation, the entire surface is blue, as expected due to the positive charge of this species.

3.5. Atomic charges and molecular electrostatic potentials of diprotonated species.

The three different atomic charges, Merz-Kollman (MK), Mulliken, and natural population (NPA), together with the MEPs values for the diprotonated (*E/Z)* and (*Z/E)* free base, cationic and hydrochloride species of RH in aqueous solution by using the B3LYP/6-31G* method are presented in Table S2 while their behaviors can be seen in Figure S4. Mulliken and NPA charges show similar curves on S1, O2, O3, O4, N5, N6, N7, and N8 atoms of diprotonated (*E/Z)* and (*Z/E)* cationic species revealing the same behaviors for these species, however, these same charges for the free base and hydrochloride (*E/Z)* and (*Z/E)* forms show less negative values on O4 of two E/Z species than the (*Z/E)* ones. Such differences are justified because the O4 is not involved in H bonds interactions as the O3 atom (O3-H34⋯N6 interactions). Note that only the MK charges of cationic and hydrochloride (*E/Z)* and (*Z/E)* species justify the positive charges on N5 atoms of those species.

The analyses of MEP values from Table S2 only show the characteristic values expected due to the different electronegativities of atoms, which are: S > O > N while the mapped MEP surfaces show the potential sites of reaction due to their different colorations, as revealed in Figure S5. Despite the diprotonated three (*Z/E)* species of ranitidine having different and higher values than the corresponding (*E/Z)* ones, both cationic species present blue colors typical of electrophilic regions, as expected because these species are positively charged while the free bases show strong red colors and nucleophilic sites on the two O atoms of NO_2 group. In the hydrochloride species, these intense colorations are evidenced on the Cl atoms and NO_2 groups (orange colors) and, in particular, in the (*Z/E)* species, both sites are closer, while in the (*E/Z)* there is a higher separation between these nucleophilic sites.

3.6. Bond orders of mono and diprotonated species.

Bond orders (BO) expressed as Wiberg bond index, totals by S, O, and N atoms were calculated for the mono and diprotonated species of ranitidine in gas and aqueous solution by using the B3LYP/6-31G* method. The results only for those atoms are presented in Table S3, while Figure S6 are shown their behaviors in both media. In the three monoprotonated species, similar curves are evidenced. Hence, similar behaviors are expected in the three species, except N5 atoms containing the dimethylamino groups, which are positively charged in the cationic and hydrochloride species. Thus, the cationic species reveal a higher BO value of N5 in solution, while the free base species in the gas phase has the same BO value as the cationic one in this medium, indicating that this latter form is not protonated. Besides, the hydrochloride species in both media present practically the same BO values. If now are analyzed the graphics of Figure S7 for the diprotonated species, similar behaviors are observed in the three species, but different BO values are observed in the O3, N5, N6, N7, and N8 atoms. An exhaustive analysis shows that the O3 atoms of NO_2 groups are forming H bonds in the three species; thus, in the (*E/Z*) forms are observed C6-H34⋯O3 bonds, while in the (*Z/E*) species are observed C7-H35⋯O3 bonds (See figure 2). Then, the differences in the BO values of N6, N7, and N8

atoms are attributed to the existence of CH_2 groups between the nitro and HNCNH-CH_3 groups. As shown in section 3.3, the different intra-molecular interactions observed in the three diprotonated (*E/Z)* species can be seen in Figure 6. These studies support the clear differences among the mono and diprotonated species of ranitidine.

3.7. Stabilities of mono and diprotonated species.

The energy values (E2) calculated for the donor-acceptor transitions from Second-Order Perturbation Theory Analysis of Fock Matrix in NBO Basis with the NBO program are parameters necessary to evaluate the stabilities of mono and diprotonated ranitidine species in different media [27]. Hence, the main delocalization energies for mono and diprotonated species of ranitidine in gas and aqueous solution by using the B3LYP/6-31G* method are presented in Table S4. Thus, the monoprotonated species show a higher number of interactions (seven) than the diprotonated ones (four) which are $\Delta E_{\pi\rightarrow\pi^*}$, $\Delta E_{\sigma\rightarrow LP^*}$, $\Delta E_{LP\rightarrow\pi^*}$, $\Delta E_{LP\rightarrow\sigma^*}$, $\Delta E_{LP\rightarrow LP^*}$, $\Delta E_{\sigma\rightarrow LP^*}$ and $\Delta E_{\pi^*\rightarrow\pi^*}$ interactions where the transitions with higher energy values are the $n\rightarrow\pi^*$ ($\Delta E_{LP\rightarrow\pi^*}$). These transitions are performed from lone pairs of O2, O3, N6, N7, and C19 atoms to antibonding orbitals of C=C bonds of furan and enamine groups, of N-O bonds of nitro groups, and N-C bonds of enamine groups. Therefore, the analyses of total energies evidence that monoprotonated cationic and hydrochloride species are the most stable in solution with values respectively of 2301.93 and 4455.46 kJ/mol in aqueous solution while the monoprotonated free base species show a total energy value in solution of 1951.43 kJ/mol, slightly lower than the cationic one in the same medium. Concerning the diprotonated species, the $n\rightarrow\pi^*$ transitions present in the three species of RH have higher energy values than the other three $n\rightarrow\sigma^*$, $n\rightarrow n^*$ and $\pi^*\rightarrow\pi^*$ interactions. This way, the total energy values show that the diprotonated (*Z/E*) cationic (933.90 kJ/mol) and hydrochloride (1350.31 kJ/mol) species are the most stable than the (*E/Z*) ones, while the free base species of both forms are the most unstable in solution. These NBO results justify the presence of diprotonated (*Z/E*) cationic and hydrochloride species in solution due to their high stabilities and confirm its presence as was experimentally observed by Cholerton *et al*. [20].

Also, the stabilities of all mono and diprotonated species of RH and the investigations of different H bonds and intra-molecular interactions were studied using the topological properties using Bader's theory of atoms in molecules [28,29]. Thus, the AIM 2000 program were calculated the electron density $\rho(r)$, the Laplacian values, $\nabla^2\rho(r)$, the eigenvalues $(\lambda1, \lambda2, \lambda3)$ of the Hessian matrix, and the $|\lambda1|/\lambda3$ ratio in the bond critical points (BCPs) and ring critical points (RCPs). In particular, if $\lambda1/\lambda3 < 1$ and $\nabla^2\rho(r) > 0$, hydrogen bonding or ionic interactions are observed. Hence, Tables S5, S6, and S7 summarize the topological properties for mono and diprotonated (*E/Z*) and (*Z/E*) species of RH calculated in the BCPs and RCPs in the gas phase and aqueous solution, respectively, by using the B3LYP/6-31G* method. Whereas Figures S8, S9, and S10 are shown the molecular models for the mono and diprotonated free base, cationic, and hydrochloride species of ranitidine in the gas phase and aqueous solution showing the geometries of critical bond points (BCPs), ring critical points (RCPs) and cage critical points (CCP) at the B3LYP/6-31G* level of theory. Analyzing Table S5 and Figure S8 corresponding to the monoprotonated species in the gas phase, in the free base, is observed three BCPs in red colors (N7-H39···O3, N6-H38···S1, and C9-H22···H43) and only three new RCPs in yellow colors named, RCPN. The RCP of the furan ring is named RCP. The cationic species shows seven BCPs (N6-H34···O3, N6-H34···S1, N8-O3···H33,

N8-O3···H43, N8-O4···H31, N8-O4···H41 and C16-H30···C20), eight RCPNs and one CCP in green color while the hydrochloride species also present one CCP, eight H bonds similar to cationic ones except for new N5-H44···Cl45 interaction and eight RCPNs. Then, in the diprotonated (*E/Z)* free base in an aqueous solution are observed one H bond (O3-H34···N6) and one RCPN while the cationic species have six H bonds (N5-H44···O4, N6-H34···O3, N8-O3···H21, N8-O3···H42, C15-H26···O2, and C16-H29···H23), seven RCPNs and one CCP. It is necessary to clarify that in the free base, the N8-O3···H34 interaction is covalent due to the negative $\nabla^2\rho(r)$ and high $\lambda 1$, $\lambda 2$, $\lambda 3$ values and to the short distance between O3 and H34 atoms (1.021 Å) while the new H bond formed is between the NO-H of NO_2 group and N-H bond. In the cationic species, it is observed that the O atoms of the NO_2 group form the N5-H44···O4, N8-O3···H21, and N8-O3···H42 interactions where the first of them presents the higher density. The hydrochloride species shows only three H bonds (N5-H44···Cl45, O3-H34···N6, and C17-H33···O2) and two RCPNs. Concerning the diprotonated (*Z/E*) species, the three species show eight new H bonds and one CCPs but the free base evidence eight RCPNs while seven RCPNs the cationic and only six RCPNs the hydrochloride one. Hence, the three diprotonated (*Z/E*) species are more stable in aqueous solution than the (E/Z) and the monoprotonated ones in the gas phase, except hydrochloride species monoprotonated of RH that also is stable in the gas phase.

3.8. Frontier HOMO-LUMO studies.

The difference between the HOMO and LUMO electronic levels, known as the energy gap, is an interesting parameter to predict theoretically the reactivity and kinetic stability of a species [30,31]. Moreover, the behaviors of species can also be evaluated by using diverse descriptors of reactivity, such as global hardness (η), global softness (S), and global electrophilicity index (ω) [23-26,44-52]. Thus, HOMO and LUMO, energy band gap, was calculated for the mono and diprotonated (E/Z) and (Z/E) species of ranitidine in the gas phase and aqueous solution using the hybrid B3LYP/6-31G*level of the theory are presented in Table S8. A quick observation of the table shows that all mono and diprotonated hydrochloride species are the most reactive in both media because they have low energy gap values (3.5348-3.0042 eV) being the most reactive in the diprotonated (*Z/E*) form while the diprotonated cationic (*E/Z*) and (*Z/E*) are the less reactive in solution. The species with a higher gap value have a higher global hardness (η), while those with a low gap have a higher global softness (*S*). On the other side, only the cationic species present a higher electrophilicity index (ω), as evidenced by the blue colors typical of electrophilic regions by the mapped MEP surfaces because these species are positively charged.

3.9. Vibrational study.

The monoprotonated RH in the gas phase was optimized with C_1 symmetry and presents 129 vibration modes, while the diprotonated (*E/Z*) and (*Z/E*) ones were also optimized in an aqueous solution with that symmetry, but due to the presence of another H atom in these species 132 vibration modes are expected in those two species. Then, all vibration modes present activities in both spectra. The IR spectrum of monoprotonated species was taken from Ref [53] and the Raman one from Ref [18], while the IR spectra of both diprotonated RH were taken from Ref [20]. Comparisons among the experimental IR spectrum of monoprotonated RH form corresponding to the free base, cationic, and hydrochloride species can be seen in Figure 7. The

assignments of all species of RH were performed with the SQMFF procedure, using scaling factors, normal internal coordinates, and the Molvib program [21,22]. Observed and calculated wavenumbers and assignments for the mono and diprotonated hydrochloride species of RH in the gas phase and aqueous solution are presented in Table 5. Comparisons among the experimental IR spectra for the diprotonated RH with the corresponding to the free base, cationic, and hydrochloride species in solution are shown in Figure 8, while only the diprotonated (*Z/E*) hydrochloride and free base are presented in Figure 9 because the calculations for the cationic species were predicted with imaginary frequencies.

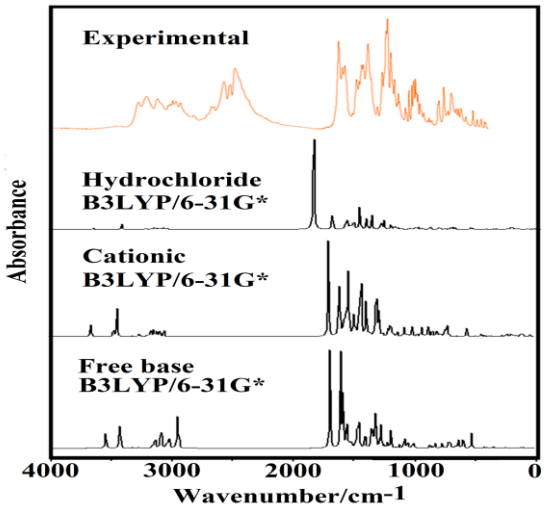


Figure 7. Experimental Infrared spectra of ranitidine hydrochloride in the solid phase [53] compared with the predicted monoprotonated free base, cationic, and hydrochloride species of ranitidine in the gas phase using the hybrid B3LYP/6-31G* method.

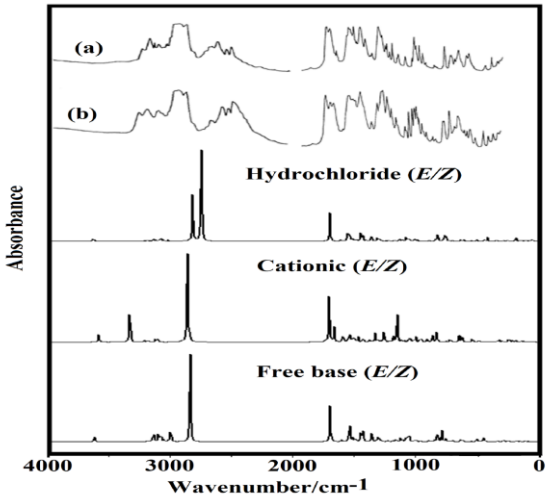


Figure 8. Comparisons among the experimental IR spectra for the diprotonated hydrochloride ranitidine [20] corresponding to the free base, cationic, and hydrochloride (*E/Z*) species in solution by using the hybrid B3LYP/6-31G* method.

Table 5. Observed and calculated wavenumbers (cm^{-1}) and assignments for the mono and diprotonated ranitidine hydrochloride in the gas phase and aqueous solution.

Experimental[a]		Monoprotonated[a]		Diprotonated E/Z[a]		Diprotonated Z/E	
		Gas-phase		Aqueous Solution			
IR[c]	Ra[d]	SQM[b]	Assignments[a]	SQM[b]	Assignments[a]	SQM[b]	Assignments[a]
3414w,br		3466	νN7-H35	3469	νN7-H35	3408	νN6-H34
3263w		3247	νN6-H34			3331	νN7-H35
3200w	3189w	3143	ν_sC-H	3147	ν_sC-H	3147	ν_sC-H
3116sh	3118w	3138	νC19-H36	3137	ν_aC-H	3136	ν_aC-H
3104w	3097w	3131	ν_aC-H				
3080w				3072	ν_aCH$_3$(C17)	3082	ν_aCH$_2$(C19)
				3069	ν_aCH$_3$(C40)	3069	ν_aCH$_3$(C40)
		3066	ν_aCH$_3$(C17)	3066	ν_aCH$_3$(C17)	3066	ν_aCH$_3$(C17)
		3064	ν_aCH$_3$(C40)	3064	ν_aCH$_3$(C40)	3065	ν_aCH$_3$(C20)
		3055	ν_aCH$_3$(C40)	3052	ν_aCH$_2$(C19)	3064	ν_aCH$_3$(C40)
		3051	ν_aCH$_3$(C17)	3045	ν_aCH$_3$(C20)	3062	ν_aCH$_3$(C17)
				3041	ν_aCH$_2$(C9)	3045	ν_aCH$_2$(C9)
		3021	ν_aCH$_3$(C20)			3028	ν_aCH$_2$(C12)
3017w	3014m	3014	ν_aCH$_2$(C9)	3022	ν_aCH$_2$(C12)	3019	ν_aCH$_2$(C15)
	3014m	3010	ν_aCH$_2$(C12)	3002	ν_aCH$_2$(C15)	3008	ν_sCH$_2$(C19)
3005w		2998	ν_aCH$_2$(C15)	3000	ν_aCH$_3$(C20)	3006	ν_aCH$_2$(C16)
2985w		2995	ν_aCH$_2$(C16)	2985	ν_sCH$_2$(C9)	3004	ν_aCH$_3$(C20)
		2982	ν_aCH$_3$(C20)	2982	ν_sCH$_2$(C19)	2987	ν_sCH$_2$(C9)
		2971	ν_sCH$_3$(C40)	2979	ν_sCH$_3$(C17)	2976	ν_sCH$_3$(C40)
	2961m	2967	ν_sCH$_3$(C17)	2975	ν_sCH$_3$(C40)	2970	ν_sCH$_2$(C12)
	2961m	2961	ν_sCH$_2$(C9)	2958	ν_sCH$_2$(C12)	2970	ν_sCH$_3$(C17)
2956w		2956	ν_sCH$_2$(C12)	2949	ν_sCH$_2$(C15)	2964	ν_sCH$_2$(C15)
	2943m	2946	ν_sCH$_2$(C15)	2939	ν_sCH$_3$(C20)	2957	ν_sCH$_2$(C16)
2921w	2920s	2924	ν_sCH$_3$(C20)	2917	ν_aCH$_2$(C16)	2942	ν_sCH$_3$(C20)
2885sh		2891	ν_sCH$_2$(C16)	2885	ν_sCH$_2$(C16)		
2810w	2814w		1428+1390= 2818		1579+1233= 2812		
2662w	2662w		1629+1032= 2661				

Experimental[a]		Monoprotonated[a]		Diprotonated E/Z[a]		Diprotonated Z/E	
		Gas-phase		Aqueous Solution			
IR[c]	Ra[d]	SQM[b]	Assignments[a]	SQM[b]	Assignments[a]	SQM[b]	Assignments[a]
2646w			1629+1016= 2645				
2563m	2549w			2718	νN6-H34		
2515m	2500w					2653	νN5-H44
2475s	2428w			2625	νN5-H44		
		1764	νN5-H44				
1629vs	1626m	1634	ρN6-H34,νC19=C18	1628	νN6=C18	1639	νN7=C18,νN6=C18
1599s		1599	νC10=C13	1601	νC10=C13	1600	νC10=C13
1579s						1568	ρN7-H35
	1554vs	1535	νC11=C14				
	1554vs	1525	$\nu_a NO_2$	1541	νC11=C14	1538	νC11=C14
1515vw		1509	νN7-C18,νN6-C18	1503	ρN6-H34		
		1491	ρN7-H35	1492	ρN5-H44	1498	ρN6-H34
1483m		1485	ρN5-H44,δN5H44Cl45				
		1473	δCH_2(C16)	1475	$\delta_a CH_3$(C20),ρN7-H35	1479	ρN5-H44,ρ'N5-H44 δN5H44Cl45
		1469	$\delta_a CH_3$(C17)	1470	ρ'N5-H44	1472	$\delta_a CH_3$(C17)
1461sh		1463	$\delta_a CH_3$(C40)				
		1459	δCH_2(C16),$\delta_a CH_3$(C20)	1459	$\delta_a CH_3$(C40)		
	1451w	1457	$\delta_a CH_3$(C40)	1452	δCH_2(C16)	1454	$\delta_a CH_3$(C17)
		1455	$\delta_a CH_3$(C20),$\delta_a CH_3$(C20)	1447	$\delta_a CH_3$(C17)	1448	δCH_2(C16)
				1446	$\delta_a CH_3$(C20)	1445	$\delta_a CH_3$(C20)
		1444	$\delta_a CH_3$(C17)	1441	$\delta_s CH_3$(C20)	1444	$\delta_a CH_3$(C40),$\delta_a CH_3$(C20)
1441m				1436	$\delta_a CH_3$(C40)	1437	$\delta_a CH_3$(C40)
	1437w	1433	δCH_2(C9)	1433	$\delta_s CH_3$(C20), $\delta_a CH_3$(C20)	1436	$\delta_a CH_3$(C40)
				1428	$\delta_a CH_3$(C17)	1432	$\delta_a CH_3$(C20)
1428m		1428	δCH_2(C12)	1428	$\delta_a CH_3$(C40), δCH_2(C9)		
				1419	δCH_2(C12),δCH_2(C9)	1423	δCH_2(C9)
		1423	ρ'N5-H44	1419	δCH_2(C12), δCH_2(C9)	1421	$\delta_a CH_3$(C40)
		1415	δCH_2(C15)	1415	δCH_2(C15)	1414	$\delta_s CH_3$(C17)
	1408w	1408	$\delta_s CH_3$(C20), $wagCH_2$(C16)			1412	$\delta_s CH_3$(C20)
		1405	$\delta_s CH_3$(C17)	1403	δCH_2(C19)	1404	δCH_2(C15)
		1401	$\delta_s CH_3$(C40)	1401	$\delta_s CH_3$(C40),$\delta_s CH_3$(C17)	1403	δCH_2(C12)
		1397	$\delta_s CH_3$(C20)	1397	$wagCH_2$(C16)	1395	$\delta_s CH_3$(C40)
1390vs		1386	$wagCH_2$(C9), νC13-C14	1394	νC19-C18	1383	$wagCH_2$(C16)
1380sh	1377w	1375	$wagCH_2$(C16)	1369	$\nu_a NO_2$	1372	νC13-C14
				1369	νC13-C14		
1366sh		1367	$wagCH_2$(C9)	1364	$wagCH_2$(C9)	1363	$wagCH_2$(C9)
						1338	ρN7-H35,νN7-C18
						1332	$wagCH_2$(C19)
		1322	$wagCH_2$(C15),νN8-C19	1316	$wagCH_2$(C19),νN7-C18	1323	$wagCH_2$(C15)
1312w		1315	$wagCH_2$(C15)	1312	ρCH_2(C16)	1309	ρCH_2(C9)
	1307w	1305	ρCH_2(C9)	1301	ρCH_2(C9)		
				1285	$wagCH_2$(C15)	1281	$wagCH_2$(C12)
1272m		1279	$wagCH_2$(C12)	1276	$wagCH_2$(C12)	1278	ρCH_2(C19)
	1262s	1253	ρC19-H36			1254	ρCH_2(C16)
	1248vs	1247	ρCH_3(C17),ρ'CH_3(C40)	1245	ρCH_2(C19)		
1241vs		1236	ρCH_2(C12), νO2-C11	1241	ρCH_3(C17), ρ'CH_3(C40)	1241	ρCH_3(C17)
1233vs	1227s	1228	ρCH_2(C16), ρC19-H36	1228	ρCH_2(C12), βC13-H25	1231	ρCH_2(C12), βC13-H25
		1217	νO2-C10			1211	ρCH_2(C15)
1203s		1203	βC14-H28,βC13-H25	1207	νO2-C10	1205	νO2-C10,βC14-H28
				1198	νC11-C12,βR_2	1198	νC11-C12,βR_2,νC9-C10
	1186s	1189	ρCH_2(C15), ρCH_2(C16)	1182	ρCH_2(C15)		
				1179	ρCH_3(C20),νN7-C20	1178	ρCH_3(C20)
1175m	1165w	1175	ρ'CH_3(C17)	1174	ρCH_3(C40),ρ'CH_3(C17)	1175	ρ'CH_3(C17)
1143m		1152	ρCH_3(C20)			1151	νsNO_2,δNO_2
1135sh	1136w	1136	ρ'CH_3(C20)	1135	ρ'CH_3(C20)	1129	ρCH_2(C12)
						1126	ρ'CH_3(C20)
1125sh		1126	ρ'CH_3(C40)	1120	ρCH_2(C12), ρ'CH_3(C40)	1120	ρ'CH_3(C40)
		1112	νN6-C16				
		1111	ρCH_2(C12)	1114	ρCH_2(C12)	1109	$\nu_a NO_2$
1083w	1072w	1079	νN7-C20	1081	δC18N6C16	1079	νN6-C16
		1065	ρCH_3(C40),ρCH_3(C17)	1062	ρCH_3(C40),ρ'CH_3(C17)		
1053m	1046w			1055	ρC18-C19, δN8C19C18	1055	ρCH_3(C40)
1032m				1029	νC15-C16	1039	νN7-C20
1016m	1023w	1020	βC13-H25,βC14-H28	1022	νN8-C19,νN6-C16		
		1008	νN5-C40,νN5-C17	1011	βC13-H25,βC14-H28	1012	βC13-H25,βC14-H28
1004m	1007w	1000	νN8-C19,$\nu_s NO_2$	1000	νN5-C17,νN5-C40	1007	νC15-C16
994m						999	νN5-C40
988sh		985	νC15-C16				

Experimental[a]		Monoprotonated[a]		Diprotonated E/Z[a]		Diprotonated Z/E	
		Gas-phase		Aqueous Solution			
IR[c]	Ra[d]	SQM[b]	Assignments[a]	SQM[b]	Assignments[a]	SQM[b]	Assignments[a]
		980	νC15-C16,νN5-C9				
972w	975w	971	νO2-C11,βR_2	968	βR_1	972	βR_1
960sh	955w			958	νO2-C11	958	νO2-C10,νO2-C11
		953	νN5-C9,βR_1	950	τwCH_2(C16)		
934w		940	τwCH_2(C16)	937	νN5-C9,νN5-C17	934	νN5-C17
				919	τwCH_2(C19)	921	τwCH_2(C19)
		908	τwCH_2(C15)			909	τwCH_2(C16)
892w	880w			878	γC13-H25	877	γC13-H25
873w		874	τwCH_2(C9)			873	τwCH_2(C9)
		863	γN6-H34	869	τwCH_2(C9)	866	νC19-C18,δN6C16C15
821sh		858	γC13-H25	848	δN8C19C18	836	νN8-C19, δN8C19C18, γC18-C19
813w		810	γC14-H28	819	τwCH_2(C12)	818	γC14-H28
	802w	801	τwCH_2(C12), γC14-H28	805	γC14-H28	799	τwCH_2(C12)
		796	τwCH_2(C12)	783	νN5-C9	788	νN5-C9
771m		768	δNO_2,δN8C19C18	776	$\nu_s NO_2$	771	τwCH_2(C15)
769sh		760	wagNO_2				
	757w	753	δN5C9C10	751	δN5C9C10,γC10-C9		
737w		750	wagNO_2	748	γN6-H34,ρN6-H34	748	δN5C9C10,γC10-C9
	720w	718	γC11-C12	738	γN6-H34,ρN6-H34	725	γC11-C12, δS1C12C11
712m		711	γC11-C12,γC18-C19	716	νS1-C15	710	γC11-C12
700sh		700	γC19-H36	695	τwCH_2(C15)	691	νS1-C12
672w	661w	686	νS1-C12,νC11-C12	685	νS1-C12		
652w		671	γC18-C19	669	δN8C19C18, wagNO_2		
630w						636	νS1-C15
622sh		629	νS1-C15	610	τR_1,γC11-C12	622	γN7-H35,νS1-C15
		607	τR_2,γC10-C9	602	τR_2	606	τR_2
592w		600	τR_1	600	δN6C18N7	593	τR_1
						579	τC18-N6, δNO_2
	583w	554	γN7-H35	573	γC18-C19	564	γN7-H35,wagNO_2 δN6C18N7
534w		529	νC9-C10	521	δC9N5C40,νC9-C10	523	δC18N6C16
527sh	522w			517	wagNO_2, δNO_2	518	δC9N5C40,δC9N5C17
500w						491	γN6-H34,ρC18-C19
471w				478	wagNO_2,ρC18-C19	472	ρNO_2
459sh	457w	459	δN6C16C15, δS1C15C16				
439w						429	γN6-H34
431sh	422w	432	δC17N5C40	423	βC10-C9,δC9N5C17	425	δC17N5C40γN6-H34
421sh		413	ρNO_2, δN6C18N7	418	δC17N5C40	417	δC17N5C40,βC10-C9
		405	δC9N5C17,δC9N5C40	408	ρNO_2		
				396	γN7-H35	383	δS1C15C16
	377w	376	ρC18-C19				
		360	βC11-C12,βC10-C9	366	βC11-C12	366	βC11-C12
	353m	339	δC18N7C20,δC18N6C16	344	δS1C12C11		
	324w	333	δS1C12C11	320	νN6-H34,ρC18-C19	334	γC11-C12, δS1C12C11
	301w	293	τC16-C15	312	νN6-H34, wagNO_2	304	τC16-C15
	277w	263	τ_wC12-C11,βC11-C12	264	νN6-H34	271	τS1-C12,βC10-C9
	248w			252	νN6-H34,τwNO_2	261	δC18N7C20
		241	δC12S1C15	237	τwCH_3(C40), τwCH_3(C17)	238	τwCH_3(C17)
				230	τC16-C15	228	τC18-N7,τwCH_3(C17)
		227	νH44-Cl45	224	γN6-H34,τC18-N6	221	τC18-N7,τC18-N6
		215	τC15-S1,νH44-Cl45	217	ρC18-C19,γN6-H34		
		202	τwCH_3(C17)	214	τwCH_3(C17),τwCH_3(C40)	210	τwCH_3(C40)
		193	τC15-S1,τC16-C15			190	δS1C15C16,τC15-S1
				183	τwCH_3(C20)		
		176	τC18-N6,τC18-N7			173	τC18-N6
	164w			169	τC15-S1	165	τN6-C16,τC15-S1
		157	τwCH_3(C40)	158	νH44-Cl45	157	νH44-Cl45
		152	τC19-C18				
		144	τwCH_3(C20)			146	τC18-N7
	135sh					139	τC15-S1, δS1C12C11
		124	τC18-N6	125	τC18-N7,τC18-N6	125	τC9-N5
	115sh	115	τC15-S1,γC11-C12	117	τC18-N7,τC18-N6	113	τwCH_3(C20)
		106	τC9-N5	108	τC18-N7,τC18-N6		
		98	C18-N7,τC18-N6	105	δN5H44Cl45,τ_wC9-C10	96	τwNO_2
	82vs	86	τC18-N7	87	τC18-N6,τC18-N7	92	τ_wC9-C10
		84	τwNO_2				
	82vs	75	τ_wC12-C11,τC15-S1	76	τC18-N6,τwNO_2	80	τC18-N6,τN6-C16

Experimental[a]		Monoprotonated[a]		Diprotonated E/Z[a]		Diprotonated Z/E	
		Gas-phase		Aqueous Solution			
IR[c]	Ra[d]	SQM[b]	Assignments[a]	SQM[b]	Assignments[a]	SQM[b]	Assignments[a]
		66	τ_wC9-C10	71	τC18-N6,τwNO$_2$	66	τ_wC12-C11
		59	τC15-S1	61	τ_wC12-C11	60	τS1-C12,τ_wC12-C11
				55	τC19-C18	52	τS1-C12,τ_wC12-C11
		41	τ_wC9-C10,τS1-C12	49	τN5-H44	46	τC19-C18,τN5-H44
		40	τS1-C12,τN5-H44	36	γN6-H34	39	τS1-C12
				32	τC19-C18,γN6-H34	34	τN6-C16
		29	τN6-C16	27	τC9-N5		
		19	τ_wC12-C11	18	τC18-N6,τC18-N7,τN6-C16	23	τS1-C12,τN6-C16
		9	τS1-C12	10	τwNO$_2$,τS1-C12	21	τ_wC12-C11,τC18-N6

Abbreviations: ν, stretching; wag, wagging; τ, torsion; ρ, rocking; τw, twisting; δ, deformation; a, antisymmetric; s, symmetric. [a]This work, [b]From scaled quantum mechanics force field B3LYP/6-31G* method, [c]From Ref [53], [d]From Ref [18].

Comparisons among the three experimental IR spectra of RH in the solid phase with the corresponding predicted for the diprotonated hydrochloride (*E/Z*) and (*Z/E*) species in solution in 4000-2000 and 2000-400 cm^{-1} regions are shown in Figures S11 and S12, respectively [20,53]. Quick examinations of table 5 and figure 7 show that the νN5-H44 stretching mode is predicted in the monoprotonated form of RH at 1764 cm$^{-1,}$ but in the experimental IR spectrum, there are no bands in that region confirming the presence of cationic species in the solid phase, as was reported in diverse hydrochloride drugs with pharmacological activities [19]. If now are analyzed the IR spectra of diprotonated hydrochloride and cationic (*E/Z*) species from figure 8, the predicted spectrum for the hydrochloride one presents two intense bands at 2718 and 2625 cm^{-1}, as was observed in the experimental spectra of both diprotonated forms reported by Cholerton *et al*. [20]. In the other diprotonated cationic and free base (*E/Z*) species, very strong IR bands are predicted by SQMFF calculations in approximately 2700 cm^{-1}.

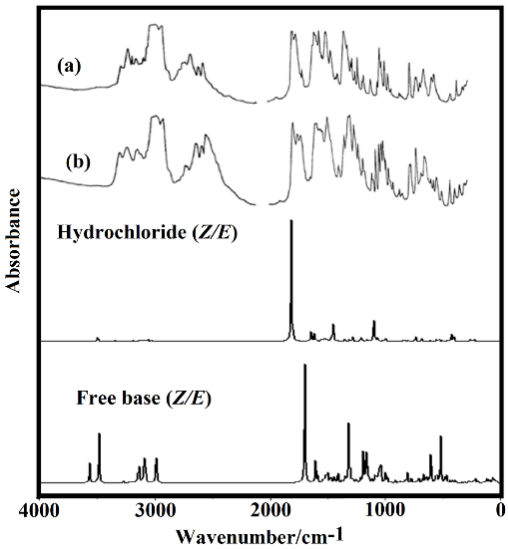


Figure 9. Comparisons among the experimental IR spectra for the diprotonated hydrochloride ranitidine [20] corresponding to the free base and hydrochloride (*Z/E*) species in solution using the hybrid B3LYP/6-31G* method.

Hence, in the solution will be present the free base is a protonated cationic species and the hydrochloride one. Here, the assignments by using the force fields of both diprotonated hydrochloride (*E/Z*) and (*Z/E*) forms by using the SQMFF methodology show clear differences because in (*E/Z*), two bands at 2718 and 2625 cm^{-1} are observed while in the (*E/Z*) species two N-H stretching modes are observed in the region of higher wavenumbers. The formation of

O3-H34···N6 bond in the (*E/Z*) form different from the (*Z/E*) one, as suggested by AIM calculations (see tables S6), justifies the strong shifting of νN6-H34 stretching mode of ranitidine towards the lower wavenumbers. Finally, analyzing comparisons of experimental spectra of both diprotonated forms reported by Cholerton *et al*. [20] from figure 9 and table 5 with the predicted hydrochloride and free base (*Z/E*) species in solution, the strong IR band at 2653 cm^{-1} is assigned to the νN5-H44 stretching mode of hydrochloride form while the other νN6-H34 and νN7-H35 stretching modes are predicted at 3408 and 3331 cm^{-1}, as predicted for the monoprotonated hydrochloride form but in reverse. The mentioned differences between the diprotonated hydrochloride (*E/Z*) and (*Z/E*) species in solution can be seen in Figures S11 and S12. Discussions of assignments of the most important groups are presented below by regions.

3.9.1. 4000-2000 cm^{-1} region.

The weak and broad band at 3414 cm^{-1} is assigned to νN7-H35 stretching modes of monoprotonated and diprotonated hydrochloride (*E/Z*) forms and also to the νN6-H34 stretching mode of diprotonated hydrochloride (*Z/E*), as predicted by SQM calculations. The weak band at 3263 cm^{-1} is assigned to νN6-H34 and νN7-H35 stretching modes of monoprotonated and diprotonated hydrochloride (*Z/E*) because the diprotonated (*E/Z*) form the νN6-H34 and νN5-H54 stretching modes are predicted at 2718 and 2625 cm^{-1}, respectively. The νN5-H54 stretching mode for the (*Z/E*) form is predicted at 2653 cm^{-1}. Thus, the IR bands at 2563, 2515, and 2475 cm^{-1} are clearly assigned to the two diprotonated species of RH. Here, the absence of an intense band at 1764 cm^{-1} in the experimental spectrum indicates that monoprotonated species are not present in the solid phase. The antisymmetric and symmetric CH_3 and CH_2 stretching modes present different assignments, as detailed in Table 5.

3.9.2. 2000-1000 cm^{-1} region.

The strong bands at 1629 and 1599 cm^{-1} are assigned to stretching modes of three RH species where the first band is assigned to C19=C18 and N6=C18 and N7=C18 stretching modes and the other one to C10=C13 stretching modes. The strong band at 1579 cm^{-1} is assigned to the in-plane deformation or rocking mode of the N7-H35 bond of hydrochloride (*Z/E*) form. Then, the very strong Raman band at 1554 cm^{-1} can be assigned to the C11=C14 stretching modes of three species of RH or the antisymmetric NO_2 mode of monoprotonated species. For the two diprotonated forms, the antisymmetric NO_2 modes are predicted at 1369 and 1109 $cm^{-1,}$ while the corresponding symmetric modes are predicted to 1000, 776, and 1151 cm^{-1} in the monoprotonated and diprotonated (*E/Z*) and (*Z/E*) forms. The low value observed for the (*E/Z*) form is due to the formation of the O3-H34···N6 bond. Table 5 can be seen in detail the assignments corresponding to C10-O2, C11-O2, C13-C14, N5-C40, N5-C17, N6-C16, N7-C20 stretching, and antisymmetric and symmetric CH_3 and CH_2 deformation, rocking and wagging modes, as predicted by calculations.

3.9.3. 1000-80 cm^{-1} region.

In this region, the differences most important between monoprotonated and diprotonated forms are observed in the NO_2 groups because the presence of O3-H34···N6 bond in the (*E/Z*) form, different from the other ones, shows different assignments for the deformation, waging, rocking and twisting modes of those groups. Hence, in the diprotonated

hydrochloride (*E/Z*) form of RH those vibration modes are assigned to lower wavenumbers, as predicted by SQMFF calculations.

The presence of H bonds in the diprotonated (*E/Z*) structures of free base, cationic, and hydrochloride species of ranitidine hydrochloride produce modifications in the positions of IR bands assigned to the NO_2 groups, as revealed in Figure 6 and, as also was observed in other species [54].

3.10. Force fields.

Scaled internal force constants of mono and diprotonated hydrochloride forms of ranitidine in the gas phase and aqueous solution using the B3LYP 6-31G* method were computed using the harmonic force fields calculated with the SQMFF methodology and the Molvib program [21,22]. Thus, the results of main scaled force constants were compared in Table 6. Analyzing the values for the $f(\nu C\text{-}H)_{Furan}$ force constants corresponding to the C-H stretching of furan rings, it is observed similar values for the three species indicate that the medium does not influence the values. However, the $f(\nu C\text{-}O)$ force constants of the same rings undergo slight differences, showing a higher value in the monoprotonated species. Such differences are justified because the C atoms of C-O bonds are linked to two different side chains. The $f(\nu C\text{-}N)$ force constant presents a higher value in the diprotonated (*E/Z*) species due to the formation of an intra-molecular H bond and, for this same reason, the $f(\nu NO_2)$ force constant of monoprotonated species has a higher value than the other ones. Moreover, due to the different side chains linked to C-S bonds, its force constants values show little difference among them, while $f(\nu CH_2)$ force constant of diprotonated (*Z/E*) species shows higher values than the other two species. Finally, the $f(\delta NO_2)$ force constant value is higher in the monoprotonated species probably because the NO_2 group is not involved in H bonds interaction, as in the diprotonated (*E/Z*) species.

Table 6. Comparison of scaled internal force constants of mono and diprotonated hydrochloride forms of ranitidine in the gas phase and aqueous solution using the B3LYP/6-31G* method.

Force constant	B3LYP/6-31G*Method[a]		
	Monoprotonated	Diprotonated *E/Z*	Diprotonated *Z/E*
	Gas Phase	Aqueous Solution	
$f(\nu C\text{-}H)_{Furan}$	5.39	5.39	5.39
$f(\nu N\text{-}H)$	6.30	4.64	6.29
$f(\nu C\text{-}O)$	5.71	4.96	5.39
$f(\nu C\text{-}N)$	5.15	5.58	5.21
$f(\nu NO_2)$	7.88	6.01	5.95
$f(\nu C\text{-}S)$	2.78	2.61	2.67
$f(\nu CH_2)$	4.88	4.89	4.98
$f(\delta NO_2)$	1.73	1.86	1.38
$f(\delta CH_2)$	0.83	0.95	0.81

Units are mdyn $Å^{-1}$ for stretching and mdyn Å rad^{-2} for angle deformations. [a]This work

4. Conclusions

This work reports a structural and vibrational study of mono and diprotonated species of potent antiacid ranitidine hydrochloride by combining B3LYP/6-31G* calculations with the SQMFF methodology. The mono and diprotonated species of ranitidine show higher dipole moment values and expansion of volumes in solution, while higher solvation energies are predicted for both diprotonated (*E/Z*) and (*Z/E*) species having higher values than the cationic ones. The presence of CH_2 groups in all diprotonated species improves the hydration in an

aqueous solution. The diprotonated three (*E/Z)* species of RH in solution present H bonds between the N-H and NO_2 groups, the (Z/E) species are most stable in this medium. The MK charges confirm positive charges on N5 atoms of cationic and hydrochloride species in both media. The bond orders support the differences among the mono and diprotonated species of ranitidine. NBO and AIM suggest high stabilities of diprotonated (*Z/E*) cationic and hydrochloride species in aqueous solution, confirming its presence, as was experimentally observed. The low energy gap values of mono and diprotonated hydrochloride species show that these species are the most reactive in both media, while the diprotonated cationic (*E/Z*) and (*Z/E*) are the less reactive in solution. In this work, the IR spectra of two polymeric forms of ranitidine hydrochloride were completely assigned, and its main force constants were reported for the first time. The diprotonated hydrochloride (*E/Z*) shows two IR bands at 2718 and 2625 cm^{-1} assigned to νN6-H34 and νN5-H44 stretching modes where the formation of O3-H34···N6 bond, different from the (*Z/E*) one, justify the strong shifting of νN6-H34 stretching mode of ranitidine towards lower wavenumbers. The IR bands at 2563, 2515, and 2475 cm^{-1} assigned to the two diprotonated species of RH, together with the absence of an intense band at 1764 $cm^{-1,}$ show clearly that monoprotonated species are not present in the solid phase, but the two diprotonated hydrochlorides (*E/Z*) and (*Z/E*) species of RH.

Funding

This work was supported with grants from CIUNT Project Nº 26/D608 (Consejo de Investigaciones, Universidad Nacional de Tucumán, Argentina).

Acknowledgments

The authors would like to thank Prof. Tom Sundius for his permission to use MOLVIB.

Conflicts of Interest

The authors declare no conflict of interest.

References

1. Available on internet: https://www.medicinenet.com/ranitidine/article.htm.
2. Grant, S.M.; Langtry, H.D.; Brogden, R.N. Ranitidine. *Drugs* **1989**, *37*, 801–870, https://doi.org/10.2165/00003495-198937060-00003.
3. Bardhan, K.D.; Bianchi Porro, G.; Bose, K.; Daly, M.; Hinchliffe, R.F.; Jonsson, E.; Lazzaroni, M.; Naesdal, J.; Rikner, L.; Walan, A. A comparison of two different doses of omeprazole versus ranitidine in treatment of duodenal ulcers. *Journal of clinical gastroenterology* **1986**, *8*, 408-413, https://doi.org/10.1097/00004836-198608000-00005.
4. Bauerfeind, P.; Cilluffo, T.; Emde, C.; Fimmel, C.; Kohler, W.; Gasser, T.; Blum, A.L. Reduction of gastric acidity with ranitidine or famotidine: early evening dosage is more effective than late evening dosage. *Digestion* **1987**, *37*, 217–222, https://doi.org/10.1159/000199504.
5. Oliva, A.; Partemi, S.; Arena, V.; De Giorgio, F.; Colecchi, C.; Fucci, N.; Pascali, V.L. Fatal injection of ranitidine: a case report. *Journal of medical case reports* **2008**, *2*, https://doi.org/10.1186/1752-1947-2-232.
6. Jain, S.; Srinath, M.S.; Narendra, C.; Reddy, S.N.; Sindhu, A. Development of a Floating Dosage Form of Ranitidine Hydrochloride by Statistical Optimization Technique. *Journal of Young Pharmacists* **2010**, *2*, 342-349, https://doi.org/10.4103/0975-1483.71619.
7. Pahwa, R.; Sharma, S.; Kumar, V.; Kohli, K. Ranitidine hydrochloride: An update on analytical, clinical and pharmacological aspects. *Journal of Chemical and Pharmaceutical Research* **2016**, *8*, 70-78.
8. Stephens, P.W.; Huq, A. Subtleties in crystal structure solution from powder data: ranitidine HCL. *Acta Cryst*. **2002**, *92*, 244-9, https://doi.org/10.1002/jps.10287.
9. Ishida, T.; In, Y.; Inoue, M. Structure of Ranitidine Hydrochloride. *Acta Cryst*. **1990**, *C46*, 1893-1896.

10. Hempel, A.; Camerman, N.; Mastropaolo, D.; Camerman, A. Ranitidine hydrochloride, a polymorphic crystal form. *Acta Cryst*. **2000**, *C56*, 1048-1049, https://doi.org/10.1107/S010827010000785X.
11. Mondal, S.; Aikat, K.; Halder, G. Optimization of ranitidine hydrochloride removal from simulated pharmaceutical waste by activated charcoal from mung bean husk using response surface methodology and artificial neural network. *Desalination and Water Treatment* **2016**, *57*, 18366-18378, https://doi.org/10.1080/19443994.2015.1088899.
12. Lanza, F.L.; Chan, F.K.; Quigley, E.M. Practice Parameters Committee of the American College of Gastroenterology. Guidelines for prevention of NSAID-related ulcer complications. *Am J Gastroenterol*. **2009**, *104*, 728-38, http://dx.doi.org/10.1038/ajg.2009.115.
13. Crowther, R.S.; Bellanger, R.; Szauter, K.E. In vitro stability of ranitidine hydrochloride in enteral nutrient formulas. *Ann Pharmacother*. **1995**, *29*, 859-62, http://dx.doi.org/10.1177/106002809502900905.
14. Demirkan, K.; Bozkurt, B.; Karakaya, G.; Kalyoncu, A.F. Anaphylactic reaction to drugs commonly used for gastrointestinal system diseases: 3 case reports and review of the literature. *J Investig Allergol Clin Immunol*. **2006**, *16*, 203-209.
15. Available on internet: https://www.fda.gov/news-events/press-announcements/fda-requests-removal-all-ranitidine-products-zantac-market.
16. Stepanova, E.V.; Arzamastsev, A.P.; Titova, A.V. Analysis of ranitidine hydrochloride by near IR spectroscopy. *Pharmaceutical Chemistry Journal* **2009**, *43*, https://doi.org/10.1007/s11094-009-0310-3.
17. Jamrógiewicz, M.; Łukasiak, J. Short Term Monitor of Photodegradation Processes in Ranitidine Hydrochloride Observed by FTIR and ATR-FTIR. *Journal of Food and Drug Analysis* **2009**, *17*, 342-347, http://dx.doi.org/10.38212/2224-6614.2591.
18. Ramesh, P.; Gunasekaran, S.; Ramkumar, G.R. Molecular Structure, Vibrational Spectra, UV-Visible and NMR Spectral Analysis on Ranitidine Hydrochloride using AB Initio and DFT Methods. *Int. J. Curr. Res. Aca. Rev*. **2015**, *3*, 117-138.
19. Brandán, S.A. Correlations in hydrochloride drugs with diverse pharmacological activities. Role of N-H···Cl bonds. *Biointerface Research in Applied Chemistry* **2020**, *10*, 5536-5547, https://doi.org/10.33263/BRIAC103.536547.
20. Cholerton, T.J.; Hunt, J.H.; Klinkert, G.; Martin-Smith, M. Spectroscopic studies on ranitidine its structure and the influence of temperature and pH. *J. Chem. Soc. Perkin Trans*. **1984**, *2*, 1761-1766, https://doi.org/10.1039/P29840001761.
21. a) Rauhut, G.; Pulay, P. Transferable Scaling Factors for Density Functional Derived Vibrational Force Fields. *J. Phys. Chem*. **1995**, *99*, 3093-3100, https://doi.org/10.1021/j100010a019.
22. Sundius, T. Scaling of ab initio force fields by MOLVIB. *Vib. Spectrosc*. **2002**, *29*, 89-95. https://doi.org/10.1016/S0924-2031(01)00189-8.
23. Ruiz Hidalgo, J.; Brandán, S.A. Theoretical DFT Studies on Free base, Cationic and Hydrochloride species of Narcotic Tramadol Agent in Gas Phase and Aqueous Solution. *Biointerface Research in Applied Chemistry* **2021**, *11*, 13064-13088, https://doi.org/10.33263/BRIAC115.1306413088.
24. Rudyk, R.A., Checa, M.A., Catalán, C.A.N., Brandán, S.A. Structural, FT-IR, FT-Raman and ECD studies on the free base, cationic and hydrobromide species of scopolamine alkaloid. *J Mol. Struct*. **2019**, *1180*, 603-617, https://doi.org/10.1016/j.molstruc.2018.12.040.
25. Márquez, M.J.; Brandán, S.A DFT study of Species Derived from the Narcotic Antagonist Naloxone. *Biointerface Research in Applied Chemistry* **2020**, *10*, 8096-8116, http://dx.doi.org/10.33263/BRIAC102.096116.
26. Guzzetti, K.A.; Iramain, M.A.; Rudyk, R.A; Manzur, M.E.; Brandán, S.A. Vibrational studies of species derived from potent S(+) and R(-) Ecstasy stimulant by using *Ab-initio* calculations and the SQM approach. *Biointerface Research in Applied Chemistry* **2020**, *10*, 6783-6809, https://doi.org/10.33263/BRIAC106.67836809.
27. Glendening, E.D.; Badenhoop, J.K.; Reed, A.D.; Carpenter, J.E.; Weinhold, F. NBO 3.1; Theoretical Chemistry Institute, University of Wisconsin; Madison, WI. **1996**.
28. Bader, R.F.W. *Atoms in Molecules, A Quantum Theory*. Oxford University Press, Oxford, **1990**.
29. Biegler-Köning, F.; Schönbohm, J.; Bayles, D. AIM2000; A Program to Analyze and Visualize Atoms in Molecules. *J. Comput. Chem.* **2001**, *22*, http://dx.doi.org/10.1002/1096-987X(20010415)22:5%3C545::AID-JCC1027%3E3.0.CO;2-Y.
30. Romani, D.; Noureddine, O.; Issaoui, N.; Brandán, S.A. Properties, Reactivities and Molecular docking of Potential Antiviral to Treatment of COVID-19 Niclosamide in different media. *Biointerface Research in Applied Chemistry* **2020**, *10*, 7295-7328, https://doi.org/10.33263/BRIAC106.72957328.
31. Sagaama, A.; Brandán, S.A.; Issa, T.B.; Issaoui, N. Searching potential antiviral candidates for the treatment of the 2019 novel coronavirus based on DFT calculations and molecular docking. *Heliyon* **2020**, *6*, https://doi.org/10.1016/j.heliyon.2020.e04640.
32. Nielsen, A.B., Holder, A.J. Gauss View 3.0, User's Reference, GAUSSIAN Inc., Pittsburgh, PA, 2000–2003.
33. Becke, A.D. Density-functional exchange-energy approximation with correct asymptotic behavior. *Phys. Rev*. **1988**, *A38*, 3098-3100, https://doi.org/10.1103/PhysRevA.38.3098.

34. Lee, C.; Yang, W.; Parr, R.G. Development of the Colle-Salvetti correlation-energy formula into a functional of the electron density. *Phys. Rev.* **1988**, *B37*, 785-789, https://doi.org/10.1103/PhysRevB.37.785.
35. Frisch, M.J.; Trucks, G.W.; Schlegel, H.B.; Scuseria, G.E.; Robb, M.A.; Cheeseman, J.R.; Scalmani, G.; Barone, V.; Mennucci, B.; Petersson, G.A. Gaussian 09, Revision A.02, M. Gaussian, Inc., Wallingford CT, **2009.**
36. Miertus, S.; Scrocco, E.; Tomasi, J. Electrostatic interaction of a solute with a continuum. *Chem. Phys.* **1981,** *55*, 117–129, https://doi.org/10.1016/0301-0104(81)85090-2.
37. Tomasi, J.; Persico, J. Molecular Interactions in Solution: An Overview of Methods Based on Continous Distributions of the Solvent. *Chem. Rev*. **1994**, *94*, 2027-2094, https://doi.org/10.1021/cr00031a013.
38. Marenich, A.V.; Cramer, C.J.; Truhlar, D.G. Universal solvation model based on solute electron density and a continuum model of the solvent defined by the bulk dielectric constant and atomic surface tensions. *J. Phys. Chem.* **2009**, *B113*, 6378-6396, https://doi.org/10.1021/jp810292n.
39. Ugliengo, P. Moldraw Program, University of Torino, Dipartimento Chimica IFM, Torino, Italy, **1998**.
40. Keresztury, G.; Holly, S.; Besenyei, G.; Varga, J.; Wang, A.Y.; Durig, J.R. Vibrational spectra of monothiocarbamates-II. IR and Raman spectra, vibrational assignment, conformational analysis and ab initio calculations of S-methyl-N,N-dimethylthiocarbamate Spectrochim. Acta **1993**, *49A*, 2007-2026, https://doi.org/10.1016/S0584-8539(09)91012-1.
41. Besler, B.H.; Merz, J.K.M.; Kollman, P.A. Atomic charges derived from semiempirical methods. *J. Comp. Chem.* **1990**, *11*, 431-439, https://doi.org/10.1002/jcc.540110404.
42. Gore, A.H.; Mote, U.S.; Tele, S.S.; Anbhule, P.V.; Rath, M.C.; Patil, S.R.; Kolekar, G.B. A novel method for ranitidine hydrochloride determination in aqueous solution based on fluorescence quenching of functionalised CdS QDs through photoinduced charge transfer process: Spectroscopic approach. *Analyst* **2011,** *136*, 2606-2612, https://doi.org/10.1039/C0AN01038C.
43. Chang, Y-X.; Qiu, Y-Q.; Du, L-M.; Li, C-F.; Guo, M. Determination of ranitidine, nizatidine, and cimetidine by a sensitive fluorescent probe. *Analyst*. **2011**, *136*, 4168-4173, https://doi.org/10.1039/c1an15078b.
44. El Kalai, F.; Karrouchi, K.; Baydere, C.; Daoui, S.; Allali, M.; Dege, N.; Benchat, N.; Brandán, S.A. Synthesis, crystal structure, spectroscopic studies, NBO, AIM and SQMFF calculations of new pyridazinone derivative. *J Mol. Struct*. **2021**, *1223*, https://doi.org/10.1016/j.molstruc.2020.129213.
45. Ruiz Hidalgo, J.; Brandán, S.A. Structural Study and Vibrational Assignments of Anticonvulsant Topiramate by using DFT calculations and Two Harmonic Force Fields. *Biointerface Research in Applied Chemistry*, **2021**, *11*, 9880-9903, https://doi.org/10.33263/BRIAC113.98809903.
46. Karrouchi, K.; Brandán, S.A.; Hassan, M.; Bougrin, K.; Radi, S.; Ferbinteanu, M.; Garcia, Y.; Ansar, M. Synthesis, X-ray, spectroscopy, molecular docking and DFT calculations of (*E*)-*N'*-(2,4-dichlorobenzylidene)-5-phenyl-*1H*-pyrazole-3-carbohydrazide. *J Mol. Struct*. **2021**, *1228*, https://doi.org/10.1016/j.molstruc.2020.129714.
47. Douche, D.; Sert, Y.; Brandán, S.A.; Kawther, A.A.; Bilmez, B.; Dege, N.; El Louzi, A.; Bougrin, K.; Karrouchi, K.; Himmi, B. 5-((1H-imidazol-1-yl)methyl)quinolin-8-ol as potential antiviral SARS-CoV-2 candidate: Synthesis, crystal structure, Hirshfeld surface analysis, DFT and molecular docking studies. *J Mol. Struct*. **2021**, *1232*, https://doi.org/10.1016/j.molstruc.2021.130005.
48. Álvarez Escalada, F.C.; Romano, E.; Brandán, S.A.; Ledesma, A.E. Experimental and computational analysis of N-Methylcytisine Alkaloid in solution. Prediction of biological activity by Docking Calculations, *Molecular Physics* **2021**, *120*, https://doi.org/10.1080/00268976.2021.1987544.
49. Vakili, M.; Romano, E.; Darugar, V.; Brandán, S.A. Behaviors of Antiviral Oseltamivir in different media. DFT and SQMFF Calculations. *J. Mol. Modeling* **2021**, *27*, https://doi.org/10.1007/s00894-021-04962-3.
50. Assenine, M.A.; Haddad, B.; Paolone, A.; Brandán, S.A.; Goussem, M.; Villemin, D.; Boumediene, M.; Rahmouni, M.; Bresson, S. Synthesis, thermal properties, vibrational spectra and computational studies of Trioctylmethylammonium bis (trifluoromethylsulfonyl) imide ionic liquid. *J Mol. Struct*. **2021**, *1232*, https://doi.org/10.1016/j.molstruc.2021.130085.
51. Fetouhi, B.; Haddad, B.; Brandán, S.A.; Paolone, A.; Villemin, D.; Boumediene, M.; Rahmouni, M.; Bresson, S. Synthesis, molecular structure, and properties of DABCO bromide based ionic liquid combining spectroscopic studies with DFT calculations. *J Mol. Struct*. **2021**, *1233*, https://doi.org/10.1016/j.molstruc.2021.130102.
52. Ouerghi, Z.; Guionneau, P.; Brandán , S.A.; Temel, E.; Kef, R. Crystal structure, computational study, optical and vibrational properties of a new luminescent material based on bismuth(III): (C10H28N4)[Bi2Cl10]. *Journal of Solid State Chemistry* **2021**, *303*, https://doi.org/10.1016/j.jssc.2021.122485.
53. Available on internet: https://spectrabase.com/spectrum/
54. Rekik, N.; Issaoui, N.; Ghalla, H.; Oujia, B.; Wójcik, M.J. Infrared spectral density of H-bonds within the strong anharmonic coupling theory: Indirect relaxation effect. *J. Mol. Struct.* **2007**, *844–845*, 21-31, https://doi.org/10.1016/j.molstruc.2007.02.040.

Supplementary Data

Table S1. Atomic charges (MK, Mulliken, NPA) for the monoprotonated species of ranitidine in gas and aqueous solution by using the B3LYP/6-31G* method.

B3LYP/6-31G*METHOD						
MONOPROTONATED						
MK	**Gas Phase**			**Aqueous Solution**		
Atoms	Free base	Cationic	Hydrochloride	Free base	Cationic	Hydrochloride
1 S	-0.165	-0.204	-0.208	-0.152	-0.146	-0.169
2 O	-0.242	-0.176	-0.198	-0.179	-0.179	-0.173
3 O	-0.530	-0.487	-0.506	-0.520	-0.580	-0.574
4 O	-0.448	-0.461	-0.450	-0.455	-0.488	-0.464
5 N	-0.185	0.190	0.814	-0.181	0.269	0.737
6 N	-0.319	-0.273	-0.404	-0.282	-0.524	-0.645
7 N	-0.424	-0.487	-0.579	-0.329	-0.499	-0.499
8 N	0.758	0.741	0.780	0.705	0.852	0.826
Mulliken	**Gas Phase**			**Aqueous Solution**		
Atoms	Free base	Cationic	Hydrochloride	Free base	Cationic	Hydrochloride
1 S	0.092	0.129	0.119	0.098	0.147	0.136
2 O	-0.472	-0.471	-0.471	-0.475	-0.483	-0.478
3 O	-0.499	-0.514	-0.483	-0.504	-0.498	-0.494
4 O	-0.440	-0.462	-0.432	-0.454	-0.463	-0.447
5 N	-0.368	-0.477	-0.467	-0.364	-0.471	-0.466
6 N	-0.670	-0.645	-0.648	-0.678	-0.653	-0.656
7 N	-0.626	-0.607	-0.610	-0.624	-0.623	-0.626
8 N	0.409	0.412	0.422	0.379	0.380	0.385
NPA	**Gas Phase**			**Aqueous Solution**		
Atoms	Free base	Cationic	Hydrochloride	Free base	Cationic	Hydrochloride
1 S	0.195	0.196	0.213	0.196	0.229	0.222
2 O	-0.459	-0.461	-0.461	-0.461	-0.468	-0.467
3 O	-0.505	-0.517	-0.501	-0.517	-0.521	-0.514
4 O	-0.430	-0.452	-0.429	-0.452	-0.472	-0.455
5 N	-0.496	-0.486	-0.485	-0.486	-0.443	-0.475
6 N	-0.645	-0.630	-0.655	-0.630	-0.632	-0.635
7 N	-0.620	-0.614	-0.630	-0.614	-0.611	-0.618
8 N	0.477	0.453	0.477	0.453	0.442	0.446
MEP	**Gas Phase**			**Aqueous Solution**		
Atoms	Free base	Cationic	Hydrochloride	Free base	Cationic	Hydrochloride
1 S	-59.176	-59.095	-59.174	-59.174	-59.092	-59.168
2 O	-22.243	-22.128	-22.230	-22.243	-22.121	-22.221
3 O	-22.340	-22.224	-22.309	-22.350	-22.239	-22.323
4 O	-22.345	-22.227	-22.312	-22.359	-22.247	-22.332
5 N	-18.343	-18.085	-18.269	-18.346	-18.070	-18.245
6 N	-18.303	-18.219	-18.299	-18.292	-18.210	-18.287
7 N	-18.314	-18.197	-18.277	-18.308	-18.191	-18.266
8 N	-18.153	-18.040	-18.123	-18.165	-18.056	-18.140

Table S2. Atomic charges (MK, Mulliken, NPA) for the diprotonated E/Z and Z/E species of ranitidine in aqueous solution by using the B3LYP/6-31G* method.

B3LYP/6-31G*METHOD						
DIPROTONATED AQUEOUS SOLUTION						
MK	**E/Z**			**Z/E**		
Atoms	Free base	Cationic	Hydrochloride	Free base	Cationic	Hydrochloride
1 S	-0.201	-0.148	-0.199	-0.201	-0.165	-0.201
2 O	-0.207	-0.130	-0.239	-0.122	-0.144	-0.142
3 O	-0.474	-0.516	-0.457	-0.518	-0.533	-0.503
4 O	-0.333	-0.519	-0.328	-0.492	-0.510	-0.520
5 N	-0.037	0.292	0.801	-0.123	0.094	0.718

6 N	-0.648	-0.464	-0.610	-0.423	-0.382	-0.423
7 N	-0.452	-0.361	-0.418	-0.446	-0.385	-0.363
8 N	0.263	0.260	0.249	0.374	0.376	0.398
Mulliken	**E/Z**			**Z/E**		
Atoms	Free base	Cationic	Hydrochloride	Free base	Cationic	Hydrochloride
1 S	0.104	0.154	0.101	0.103	0.117	0.105
2 O	-0.469	-0.482	-0.468	-0.454	-0.450	-0.449
3 O	-0.541	-0.523	-0.540	-0.509	-0.526	-0.489
4 O	-0.361	-0.532	-0.361	-0.483	-0.503	-0.495
5 N	-0.349	-0.489	-0.459	-0.348	-0.470	-0.463
6 N	-0.550	-0.569	-0.553	-0.617	-0.615	-0.618
7 N	-0.623	-0.599	-0.623	-0.573	-0.568	-0.573
8 N	0.195	0.235	0.198	0.267	0.274	0.273
NPA	**E/Z**			**Z/E**		
Atoms	Free base	Cationic	Hydrochloride	Free base	Cationic	Hydrochloride
1 S	0.206	0.249	0.204	0.189	0.203	0.193
2 O	-0.462	-0.468	-0.459	-0.448	-0.441	-0.442
3 O	-0.629	-0.608	-0.628	-0.588	-0.612	-0.574
4 O	-0.369	-0.612	-0.369	-0.543	-0.570	-0.554
5 N	-0.488	-0.468	-0.476	-0.480	-0.440	-0.471
6 N	-0.600	-0.575	-0.603	-0.592	-0.585	-0.594
7 N	-0.637	-0.575	-0.635	-0.597	-0.593	-0.598
8 N	0.271	0.308	0.271	0.311	0.321	0.317
MEP	**E/Z**			**Z/E**		
Atoms	Free base	Cationic	Hydrochloride	Free base	Cationic	Hydrochloride
1 S	-59.196	-59.089	-59.173	-59.182	-59.082	-59.159
2 O	-22.253	-22.133	-22.213	-22.268	-22.133	-22.231
3 O	-22.321	-22.255	-22.313	-22.391	-22.283	-22.375
4 O	-22.332	-22.250	-22.324	-22.392	-22.283	-22.375
5 N	-18.358	-18.130	-18.226	-18.375	-18.075	-18.246
6 N	-18.360	-18.171	-18.348	-18.269	-18.167	-18.252
7 N	-18.283	-18.145	-18.273	-18.283	-18.178	-18.267
8 N	-18.221	-18.121	-18.213	-18.246	-18.142	-18.230

Table S3. Bond orders expressed as Wiberg bond index, totals by atom for the mono and diprotonated species of ranitidine in gas and aqueous solution by using the B3LYP/6-31G* method.

B3LYP/6-31G*METHOD						
MONOPROTONATED						
Atoms	Gas Phase			Aqueous Solution		
	Free base	Cationic	Hydrochloride	Free base	Cationic	Hydrochloride
1 S	2.171	2.162	2.159	2.162	2.161	2.161
2 O	2.268	2.265	2.267	2.265	2.256	2.259
3 O	1.930	1.903	1.935	1.903	1.898	1.907
4 O	1.982	1.939	1.986	1.939	1.920	1.936
5 N	3.120	3.114	3.356	3.114	3.477	3.387
6 N	3.150	3.186	3.154	3.186	3.199	3.193
7 N	3.204	3.212	3.169	3.212	3.212	3.195
8 N	3.964	3.958	3.963	3.958	3.955	3.957
DIPROTONATED AQUEOUS SOLUTION						
Atoms	E/Z			Z/E		
	Free base	Cationic	Hydrochloride	Free base	Cationic	Hydrochloride
1 S	2.144	2.168	2.141	2.156	2.157	2.156
2 O	2.265	2.258	2.268	2.281	2.288	2.287

3 O	1.779	1.548	1.780	1.639	1.610	1.655
4 O	1.558	1.572	1.559	1.575	1.555	1.573
5 N	3.119	3.408	3.385	3.126	3.475	3.388
6 N	3.089	3.284	3.087	3.242	3.264	3.240
7 N	3.194	3.289	3.198	3.220	3.236	3.219
8 N	3.292	3.336	3.293	3.480	3.443	3.481

Table S4. Main delocalization energy (in kJ/mol) for the mono and diprotonated species of ranitidine in gas and aqueous solution using the B3LYP/6-31G* method.

B3LYP/6-31G*METHOD						
Delocalization	**MONOPROTONATED**					
	Free base		**Cationic**		**Hydrochloride**	
	Gas	PCM	Gas	PCM	Gas	PCM
πO4-N8→π O4-N8*	38.37	44.10				44.98
*πC10-C13→π*C11-C14*	67.38	66.21			62.24	60.74
*πC11-C14→π*C10-C13*	58.31	59.48			63.95	64.29
πC19-C20→π O4-N8*	157.67	199.26				
πC18-C19→π O4-N8*			103.25		158.13	
$\Delta ET_{\pi\rightarrow\pi^*}$	**321.73**	**369.05**	**103.25**		**284.32**	**170.00**
σO4-C19→LP(1)C18*				1895.09		
$\Delta ET_{\sigma\rightarrow LP^*}$				**1895.09**		
*LP(2)O2→ π*C10-C13*	118.67	113.07	55.01	53.04	113.91	111.77
*LP(2)O2→ π*C11-C14*	115.12	112.82	57.02	55.97	116.29	113.11
*LP(3)O3→ π*O4-N8*	486.93	475.77	229.02		504.19	484.67
*LP(1)N6→ π*C19-C20*	181.83	228.56				
*LP(1)N7→ π*C19-C20*	268.69	287.04				
*LP(1)N6→ π*C18-C19*			98.56		188.18	
*LP(1)N7→ π*C18-C19*			104.37		168.58	
*LP(1)N7→ π*N6-C18*						264.30
*LP(1)C19→ π*O4-N8*						2140.66
*LP(1)C19→ π*N6-C18*						753.86
$\Delta ET_{LP\rightarrow\pi^*}$	**1171.24**	**1217.26**	**543.99**	**109.01**	**1091.15**	**3868.38**
*LP(2)O3→ σ*O4-N8*	74.57	70.77			75.32	71.02
*LP(2)O3→ σ*N6-H34*					56.05	65.08
*LP(2)O3→ σ*N7-H39*	67.34	59.52				
*LP(2)O4→ σ*O3-N8*	85.02	76.79			82.60	76.41
*LP(1)N8→ σ*O4-C19*				48.99		
*LP(4)Cl45→ σ*N5-H44*					437.10	204.57
$\Delta ET_{LP\rightarrow\sigma^*}$	**226.93**	**207.08**		**48.99**	**651.08**	**417.08**
LP(1)N6→LP(1)C18*				247.92		
LP(1)N7→LP(1)C18*				231.74		
$\Delta ET_{LP\rightarrow LP^*}$				**479.66**		
*σ*O4-C19→LP*(1)C18*				130.21		
$\Delta ET_{\sigma\rightarrow LP^*}$				130.21		
*π*O4-N8→π* C19-C20*	119.30	158.05	60.11			
*π*O4-N8→π* C18-C19*					107.76	
*π*C10-C13→π*C11-C14*				248.84		
$\Delta ET_{\pi^*\rightarrow\pi^*}$	**119.30**	**158.05**	**60.11**	**248.84**	**107.76**	
ΔET_{TOTAL}	**1839.20**	**1951.43**	**707.34**	**2301.93**	**2134.31**	**4455.46**
DIPROTONATED AQUEOUS SOLUTION						
Delocalization	E/Z			Z/E		
	Free base	Cationic	Hydrochloride	Free base	Cationic	Hydrochloride
*LP(2)O2→ π*C10-C13*	56.56	54.17	55.89	57.39	55.43	
*LP(2)O2→ π*C11-C14*	57.56	55.55	57.48	59.19	58.81	
*LP(1)N7→ π*N6-C18*	131.13		132.46			179.15
*LP(1)C14→ π*O2-C11*						970.22

*LP(1)C14→ π*C10-C13*						99.73
$\Delta ET_{LP\rightarrow \pi^*}$	**245.24**	**109.73**	**245.83**	**116.58**	**114.24**	**1249.11**
*LP(3)O4→ σ*O3-N8*	57.39		57.31			
*LP(1)N6→ σ*O3-H34*	71.94		73.94			
*LP(3)O4→ σ*N5-H44*		67.84				
*LP(4)Cl45→σ*N5-H44*						101.20
$\Delta ET_{LP\rightarrow \sigma^*}$	**129.33**	**67.84**	**131.25**			**101.20**
LP(1)N6→LP(1)C18*		321.69		278.47	301.71	
LP(1)N7→LP(1)C18*		338.04		223.55	240.56	
LP(1)N5→LP(1)H44*			726.44			
LP(4)Cl45→LP(1)H44*			174.77			
$\Delta ET_{LP\rightarrow LP^*}$		**659.73**	**901.21**	**502.02**	**542.27**	
*π*C10-C13→π*C11-C14*					277.38	
$\Delta ET_{\pi^*\rightarrow \pi^*}$					**277.38**	
ΔET_{TOTAL}	**374.57**	**837.30**	**1278.29**	**618.60**	**933.90**	**1350.31**

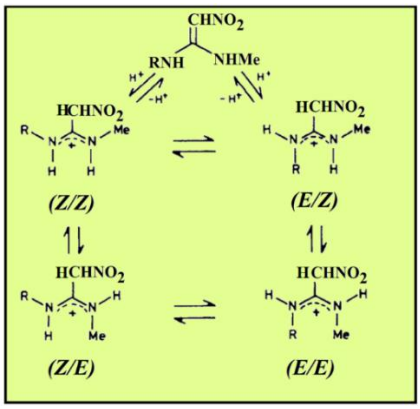


Figure S1. Scheme of protonation proposed by Cholerton *et al*. for the nitroethene group of Ranitidine [20].

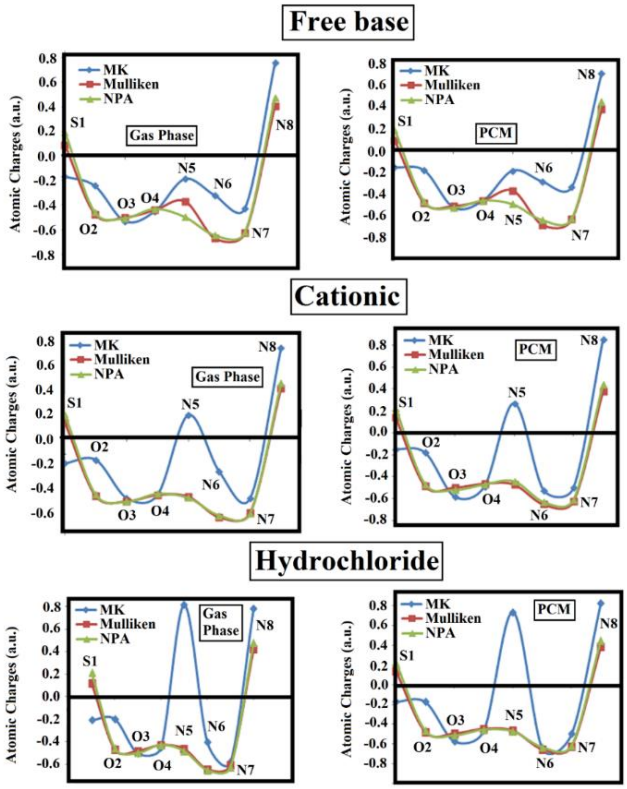


Figure S2. Calculated MK, Mulliken and NPA charges on the S1, O2, O3, O4, N5, N6, N7 and N8 atoms of monoprotonated free base, cationic and hydrochloride species of ranitidine in gas phase and aqueous solution by using B3LYP/6-31G* method.

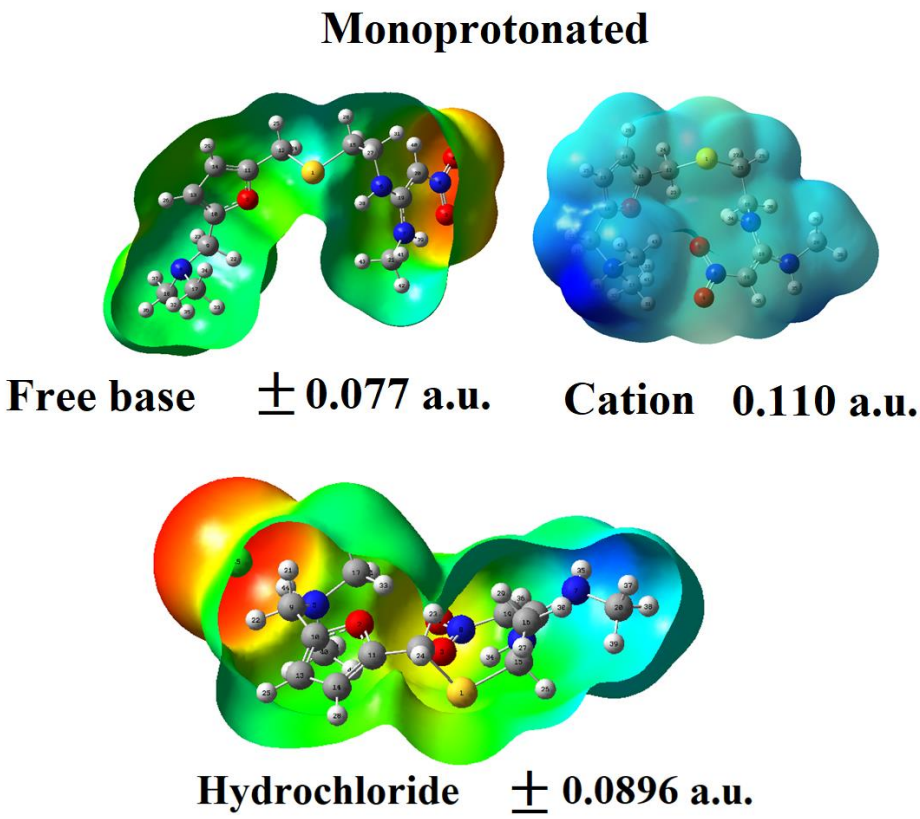


Figure S3. Calculated electrostatic potential surfaces on the molecular surface of monoprotonated free base, cationic and hydrochloride species of ranitidine in gas phase. B3LYP functional and 6-31G* basis set. Isodensity value of 0.005.

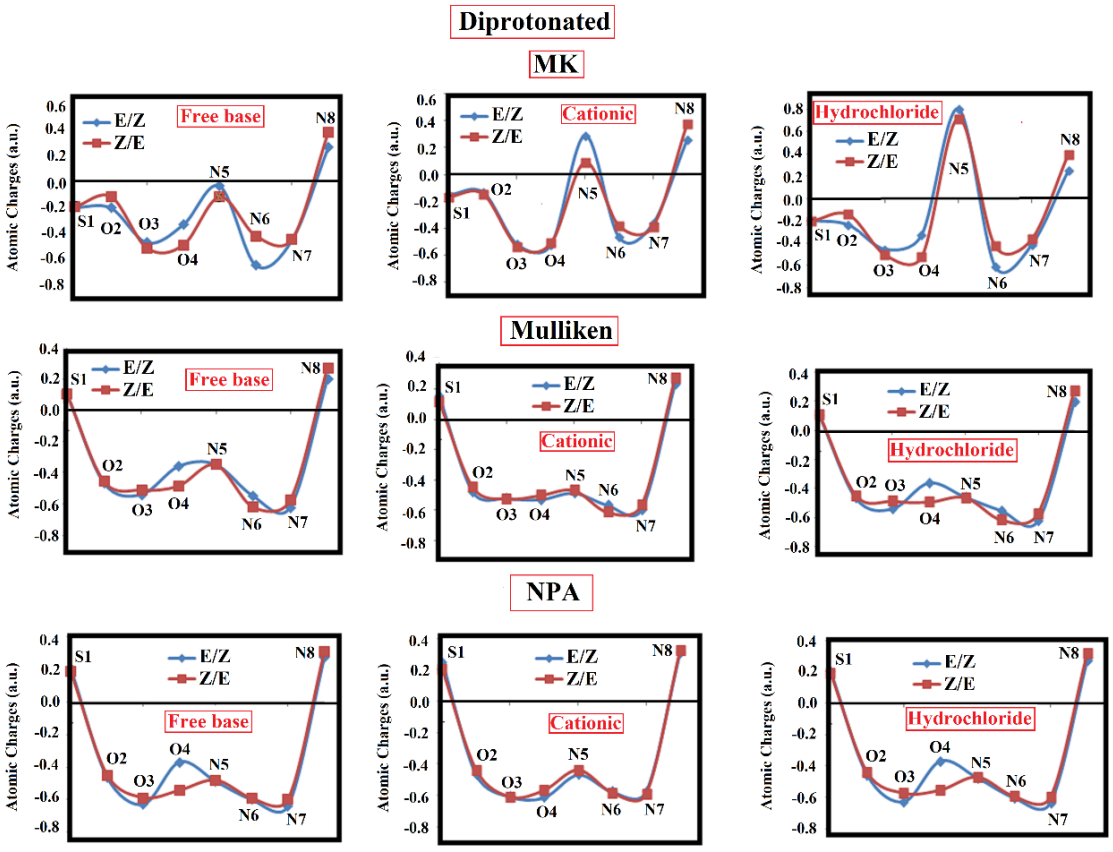


Figure S4. Calculated MK, Mulliken, and NPA charges on the S1, O2, O3, O4, N5, N6, N7, and N8 atoms of diprotonated free base, cationic, and hydrochloride species of ranitidine in aqueous solution by using B3LYP/6-31G* method.

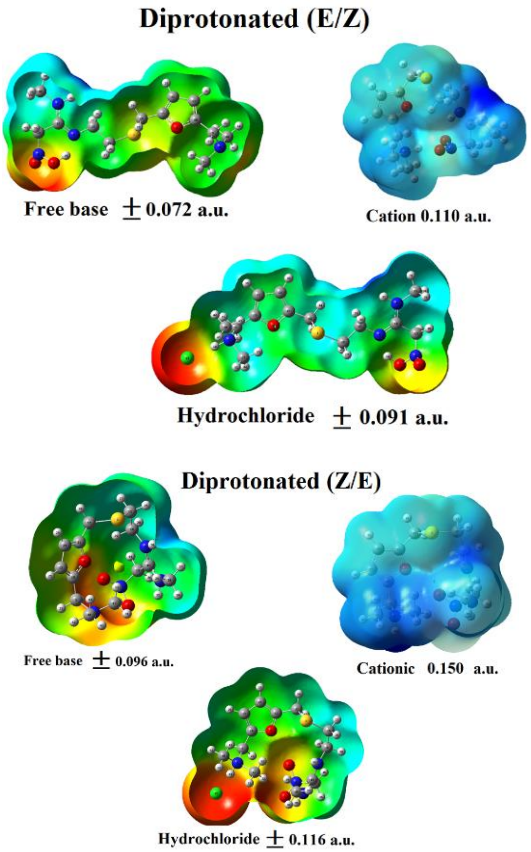


Figure S5. Calculated electrostatic potential surfaces on the molecular surface of diprotonated (*E/Z)* and (*Z/E)* free base, cationic, and hydrochloride species of ranitidine in an aqueous solution. B3LYP functional and 6-31G* basis set. Isodensity value of 0.005.

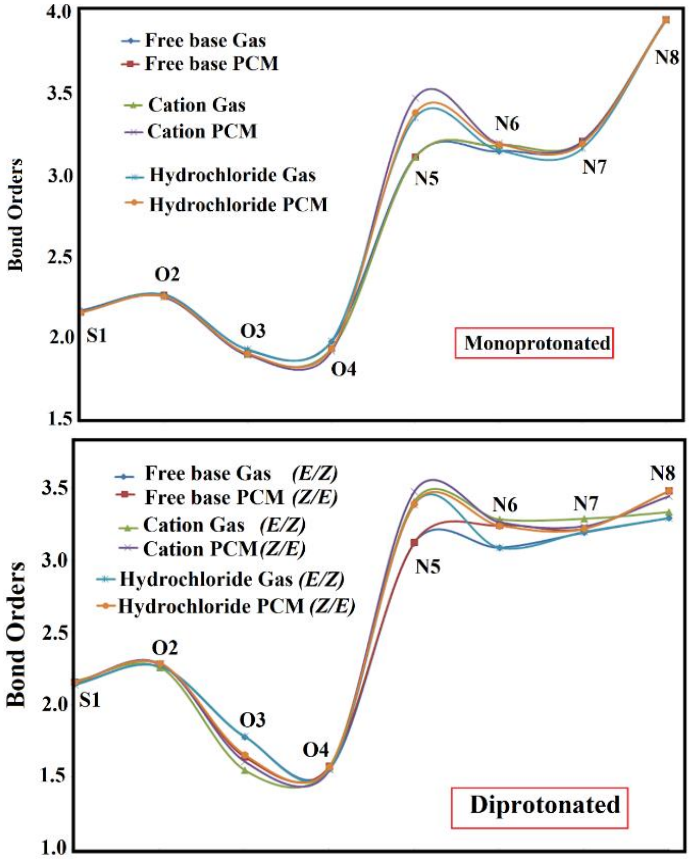


Figure S6. Bond orders of mono (upper) and diprotonated (bottom) free base, cationic, and hydrochloride species of ranitidine in the gas phase and aqueous solution by using the B3LYP/6-31G* method.

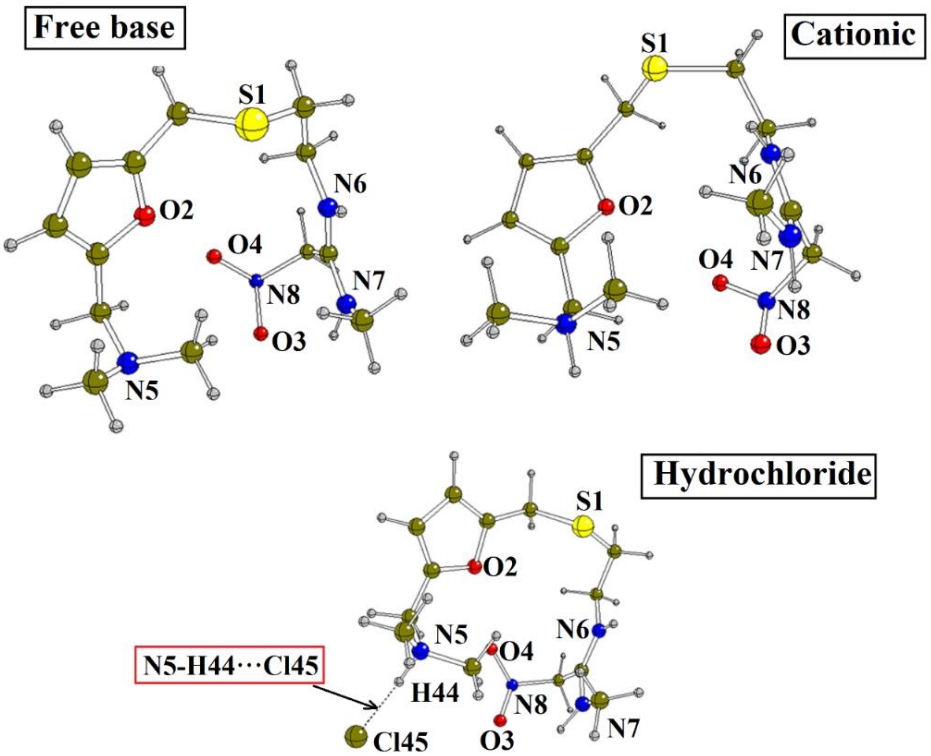


Figure S7. Optimized diprotonated free base, cationic, and hydrochloride (*Z*/*E*) species of ranitidine in an aqueous solution by using the B3LYP/6-31G* method.

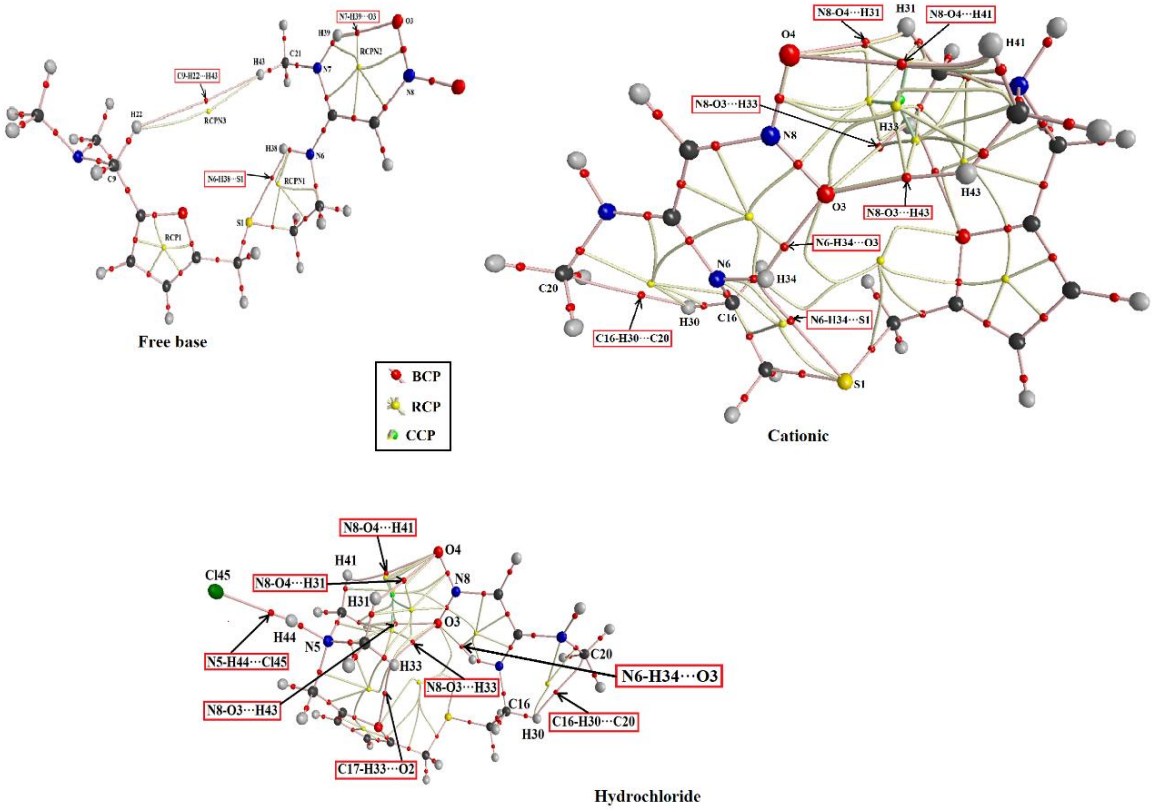


Figure S8. Details of the molecular models for the monoprotonated free base, cationic, and hydrochloride species of ranitidine in the gas phase showing the geometries of all their critical bond points (BCPs), critical ring points (RCPs) and cage critical points (CCP) at the B3LYP/6-31G* level of theory.

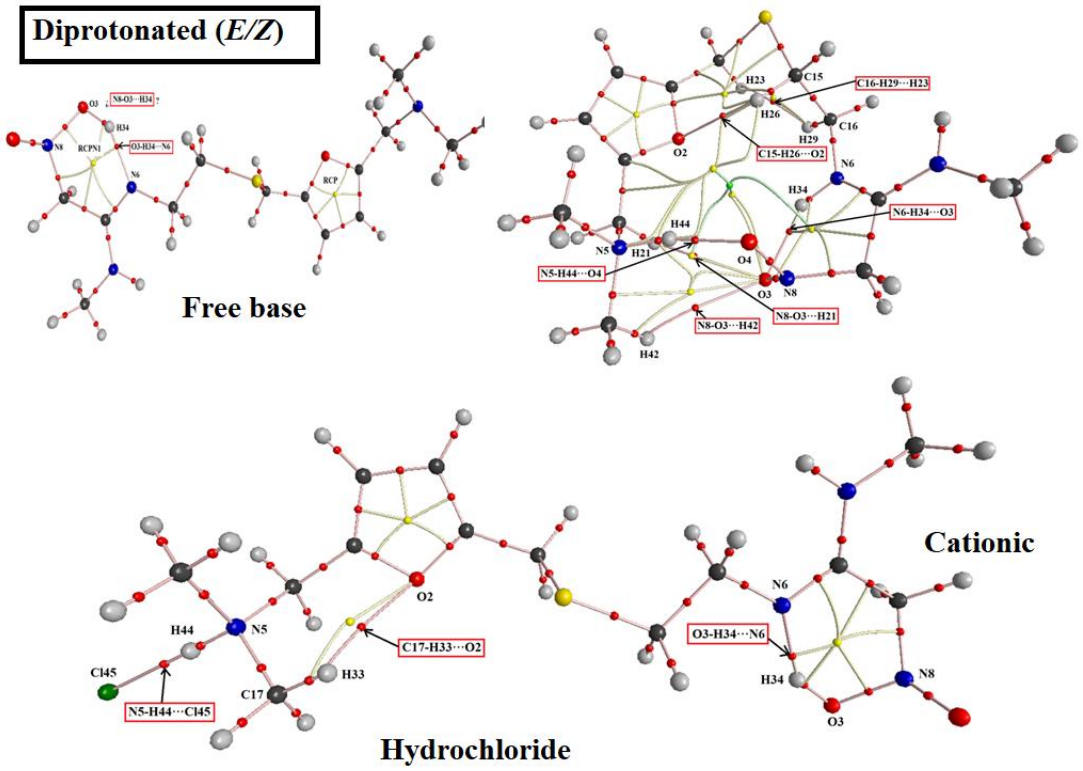


Figure S9. Details of the molecular models for the diprotonated (*E*/*Z*) free base, cationic, and hydrochloride species of ranitidine in aqueous solution showing the geometries of all their critical bond points (BCPs), ring critical points (RCPs), and cage critical points (CCP) at the B3LYP/6-31G* level of theory.

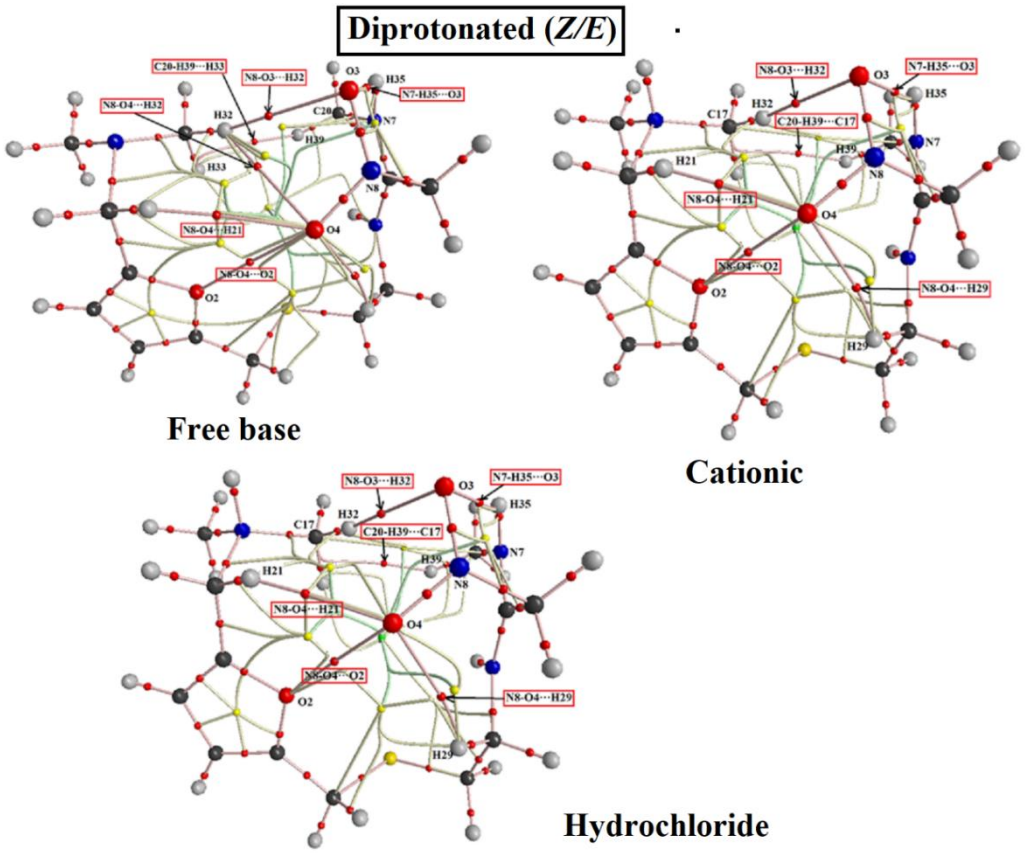


Figure S10. Details of the molecular models for the diprotonated (*Z*/*E*) free base, cationic, and hydrochloride species of ranitidine in aqueous solution showing the geometries of all their critical bond points (BCPs), ring critical points (RCPs) and cage critical points (CCP) at the B3LYP/6-31G* level of theory.

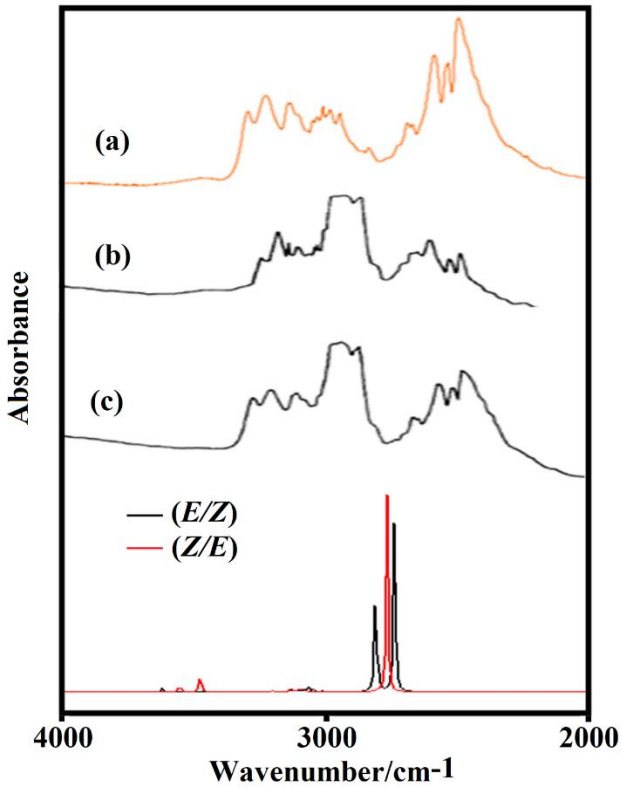


Figure S11. Experimental Infrared spectra of ranitidine hydrochloride taken between 4000 and 2000 cm^{-1} from (a) Ref [53], (b) and (c) diprotonated from Ref [20] compared with the corresponding for the (*E/Z*) and (*Z/E*) species in aqueous solution at the B3LYP/6-31G* level of theory.

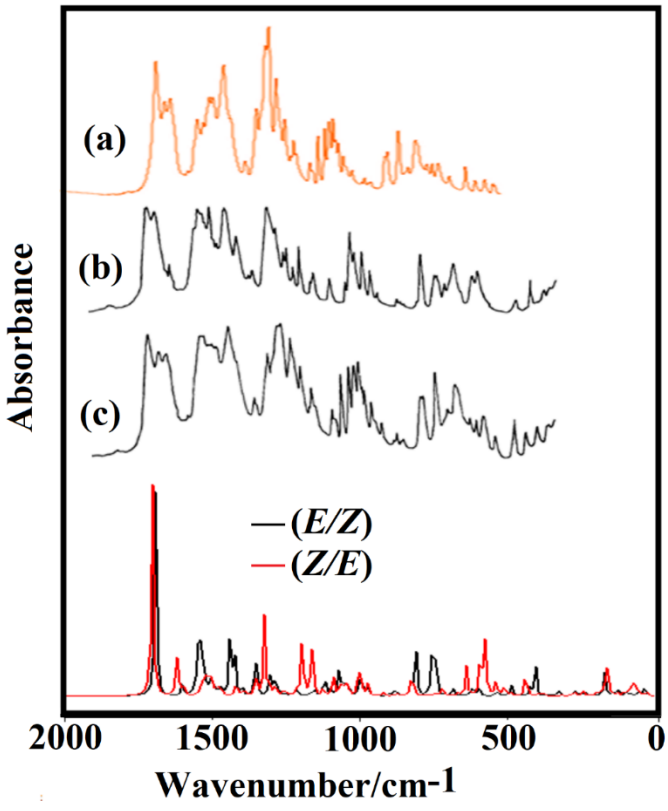


Figure S12. Experimental Infrared spectra of ranitidine hydrochloride taken between 2000 and 400 cm^{-1} from (a) Ref [53], (b) and (c) diprotonated from Ref [20] compared with the corresponding for the (*E/Z*) and (*Z/E*) species in aqueous solution at the B3LYP/6-31G* level of theory.

Table S5. Analysis of the topological properties for the monoprotonated species of ranitidine in the gas phase using the hybrid B3LYP/6-31G*level of theory.

MONOPROTONATED GAS PHASE									
Parameter (a.u.)	FREE BASE								
	N7-H39···O3	N6-H38···S1	C9-H22···H43						RCP1
$\rho(r_c)$	0.0397	0.0138	1.1114						0.0503
$\nabla^2\rho(r_c)$	0.1304	0.04932	8.4760						0.3854
λ_1	-0.0585	-0.0125	-7.0522						-0.0554
λ_2	-0.0580	-0.0074	-4.3028						0.2171
λ_3	0.2470	0.0692	9.6116						0.2237
$\lvert\lambda_1\rvert/\lambda_3$	0.2368	0.1806	0.7337						0.2477
Distance (Å)	1.808	2.615	4.959						
Parameter (a.u.)	CATIONIC								
	N6-H34···O3	N6-H34···S1	N8-O3···H33	N8-O3···H43	N8-O4···H31	N8-O4···H41	C16-H30···C20		RCP1
$\rho(r_c)$	0.0341	0.0134	0.0114	0.0141	0.0117	0.0056	0.0104		0.0502
$\nabla^2\rho(r_c)$	0.1136	0.0514	0.0407	0.0465	0.0406	0.0223	0.0432		0.3854
λ_1	-0.0489	-0.0117	-0.0116	-0.0157	-0.0120	-0.0042	-0.0082		-0.0555
λ_2	-0.0443	-0.0054	-0.0099	-0.0146	-0.0111	-0.0031	-0.0044		0.2177
λ_3	0.2069	0.0686	0.0623	0.0769	0.0637	0.0297	0.0557		0.2231
$\lvert\lambda_1\rvert/\lambda_3$	0.2363	0.1706	0.1862	0.2042	0.1884	0.1414	0.1472		0.2488
Distance (Å)	1.878	2.634	2.422	2.302	2.400	2.808	2.524		
Parameter (a.u.)	HYDROCHLORIDE								
	N6-H34···O3	N5-H44···Cl45	N8-O3···H33	N8-O3···H43	N8-O4···H31	N8-O4···H41	C16-H30···C20	C17-H33···O2	RCP1
$\rho(r_c)$	0.0351	0.0745	0.0077	0.0075	0.0070	0.0030	0.0101	0.0087	0.0502
$\nabla^2\rho(r_c)$	0.1152	0.0949	0.0288	0.0277	0.0264	0.0128	0.0428	0.0329	0.3853
λ_1	-0.0505	-0.1218	-0.0070	-0.0072	-0.0064	-0.0018	-0.0067	-0.0081	-0.0553
λ_2	-0.0473	-0.1215	-0.0060	-0.0066	-0.0060	-0.0012	-0.0041	-0.0068	0.2169
λ_3	0.2131	0.3383	0.0417	0.0415	0.0387	0.0159	0.0537	0.0479	0.2237
$\lvert\lambda_1\rvert/\lambda_3$	0.2370	0.3600	0.1679	0.1735	0.1654	0.1132	0.1248	0.1691	0.2472
Distance (Å)	1.865	1.747	2.614	2.610	2.626	3.065	2.528	2.531	

Table S6. Analysis of the topological properties for the diprotonated (*E/Z*) species of ranitidine in aqueous solution by using the hybrid B3LYP/6-31G*level of theory.

DIPROTONATED (E/Z) AQUEOUS SOLUTION							
Parameter (a.u.)	FREE BASE						
	N8-O3···H34	O3-H34···N6					RCP1
$\rho(r_c)$	0.2959	0.0545					0.0494
$\nabla^2\rho(r_c)$	-1.3952	0.1410					0.3800
λ_1	-1.4115	-0.0919					-0.0542
λ_2	-1.3766	-0.0892					0.2126
λ_3	1.3929	0.3221					0.2216
$\lvert\lambda_1\rvert/\lambda_3$	1.0134	0.2853					0.2446
Distance (Å)	1.021	1.696					
Parameter (a.u.)	CATIONIC						
	N5-H44···O4	N6-H34···O3	N8-O3···H21	N8-O3···H42	C15-H26···O2	C16-H29···H23	RCP1
$\rho(r_c)$	0.0490	0.0327	0.0046	0.0056	0.0085	0.0072	0.0496
$\nabla^2\rho(r_c)$	0.1344	0.0982	0.0188	0.0225	0.0318	0.0301	0.3817
λ_1	-0.0832	-0.0441	-0.0034	-0.0046	-0.0076	-0.0064	-0.0545
λ_2	-0.0787	-0.0429	-0.0014	-0.0031	-0.0066	-0.0019	0.2146
λ_3	0.2963	0.1853	0.0236	0.0302	0.0460	0.0385	0.2216
$\lvert\lambda_1\rvert/\lambda_3$	0.2808	0.2380	0.1441	0.1523	0.1652	0.1662	0.2459
Distance (Å)	1.713	1.892	2.886	2.795	2.560	2.236	
Parameter (a.u.)	HYDROCHLORIDE						
	N5-H44···Cl45	O3-H34···N6	C17-H33···O2				RCP1
$\rho(r_c)$	0.0452	0.0553	0.0071				0.0497
$\nabla^2\rho(r_c)$	0.0799	0.1428	0.0285				0.3816
λ_1	-0.0596	-0.0940	-0.0052				-0.0546
λ_2	-0.0595	-0.0911	-0.0027				0.2152
λ_3	0.1991	0.3280	0.0364				0.2209
$\lvert\lambda_1\rvert/\lambda_3$	0.2993	0.2866	0.1429				0.2472
Distance (Å)	1.991	1.689	2.681				

Table S7. Analysis of the topological properties for the diprotonated (*Z/E*) species of ranitidine in aqueous solution by using the hybrid B3LYP/6-31G*level of theory.

DIPROTONATED (*Z/E*) AQUEOUS SOLUTION							
Parameter (a.u.)	FREE BASE						
	N7-H35···O3	N8-O3···H32	N8-O4···H21	N8-O4···H32	N8-O4···O2	C20-H39···H33	RCP1
$\rho(r_c)$	0.0206	0.0062	0.0053	0.0043	0.0043	0.0033	0.0495
$\nabla^2\rho(r_c)$	0.0606	0.0216	0.0197	0.0177	0.0194	0.0118	0.3804
λ_1	-0.0239	-0.0059	-0.0050	-0.0036	-0.0039	-0.0023	-0.0543
λ_2	-0.0213	-0.0057	-0.0046	-0.0019	-0.0033	-0.0013	0.2130
λ_3	0.1058	0.0333	0.0294	0.0232	0.0267	0.0155	0.2217
$\lvert\lambda_1\rvert/\lambda_3$	0.2259	0.1772	0.1701	0.1552	0.1461	0.1484	0.2449
Distance (Å)	2.149	2.697	2.749	2.861	3.194	2.673	

Parameter (a.u.)	CATIONIC						
	N7-H35···O3	N8-O3···H32	N8-O4···H21	N8-O4···H29	N8-O4···O2	C20-H39···C17	RCP1
$\rho(r_c)$	0.0200	0.0114	0.0097	0.0049	0.0054	0.0036	0.0499
$\nabla^2\rho(r_c)$	0.0600	0.0326	0.0308	0.0192	0.0224	0.0142	0.3829
λ_1	-0.0230	-0.0124	-0.0102	-0.0040	-0.0049	-0.0026	-0.0549
λ_2	-0.0203	-0.0118	-0.0095	-0.0020	-0.0040	-0.0015	0.2154
λ_3	0.1033	0.0568	0.0506	0.0252	0.0313	0.0183	0.2223
$\lvert\lambda_1\rvert/\lambda_3$	0.2227	0.2183	0.2016	0.1587	0.1565	0.1421	0.2470
Distance (Å)	2.013	5.000	4.660	2.479	3.036	6.811	
Parameter (a.u.)	HYDROCHLORIDE						
	N5-H44···Cl45	N7-H35···O3	N8-O3···H32	N8-O4···H21	N8-O4···O2	C20-H39···H22	RCP1
$\rho(r_c)$	0.0443	0.0212	0.0100	0.0061	0.0048	0.0042	0.0498
$\nabla^2\rho(r_c)$	0.0794	0.0621	0.0314	0.0226	0.0206	0.0160	0.3822
λ_1	-0.0582	-0.0249	-0.0106	-0.0060	-0.0042	-0.0033	-0.0548
λ_2	-0.0581	-0.0224	-0.0102	-0.0055	-0.0037	-0.0022	0.2156
λ_3	0.1957	0.1095	0.0522	0.0341	0.0286	0.0215	0.2215
$\lvert\lambda_1\rvert/\lambda_3$	0.2974	0.2274	0.2031	0.1760	0.1469	0.1535	0.2474
Distance (Å)	1.999	2.131	2.465	2.675	3.161	6.216	

Table S8. Calculated HOMO and LUMO orbitals, energy band gap, global hardness (η), global softness (S), and global electrophilicity index (ω) for the mono and diprotonated (*E*/*Z*) and (*Z*/*E*) species of ranitidine in the gas phase and aqueous solution by using the hybrid B3LYP/6-31G*level of theory.

B3LYP/6-31G* method[a]									
Frontier orbitals (eV)	**GAS PHASE**			**AQUEOUS SOLUTION**					
	Monoprotonated			**(*E*/*Z*)**			**(*Z*/*E*)**		
	Free base	Cationic	Hydrochloride	Free base	Cationic	Hydrochloride	Free base	Cationic	Hydrochloride
HOMO	-5.6709	-8.7022	-5.2055	-5.7117	-8.8682	-4.9661	-5.0314	-8.0192	-4.3729
LUMO	-0.8680	-4.1633	-1.8721	-1.2245	-4.2042	-1.4313	-0.9415	-3.8014	-1.3687
|GAP|	4.8029	4.5389	**3.3334**	4.4872	4.6640	**3.5348**	4.0899	4.2178	**3.0042**
Descriptors (eV)									
h	2.4015	2.2695	1.6667	2.2436	2.3320	1.7674	2.0450	2.1089	1.5021
S	0.2082	0.2203	0.3000	0.2229	0.2144	0.2829	0.2445	0.2371	0.3329
w	2.2256	9.1168	3.7569	2.6805	9.1599	2.8946	2.1807	8.2820	2.7433

$\eta = [E(LUMO) - E(HOMO)]/2$; $S = \frac{1}{2}\eta$; $\omega = \mu^2/2\eta$

[a]This work